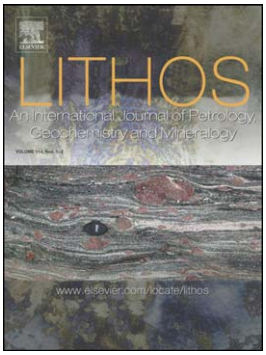

Paradoxical co-existing base metal sulphides in the mantle: The multi-event record preserved in Loch Roag peridotite xenoliths, North Atlantic Craton

Hannah S.R. Hughes, Iain McDonald, Matthew Loocke, Ian B. Butler, Brian G.J. Upton, John W. Faithfull

PII: S0024-4937(16)30328-0
DOI: doi:10.1016/j.lithos.2016.09.035
Reference: LITHOS 4097

To appear in: *LITHOS*

Received date: 15 May 2016
Revised date: 7 September 2016
Accepted date: 28 September 2016

Please cite this article as: Hughes, Hannah S.R., McDonald, Iain, Loocke, Matthew, Butler, Ian B., Upton, Brian G.J., Faithfull, John W., Paradoxical co-existing base metal sulphides in the mantle: The multi-event record preserved in Loch Roag peridotite xenoliths, North Atlantic Craton, *LITHOS* (2016), doi:10.1016/j.lithos.2016.09.035

Paradoxical co-existing base metal sulphides in the mantle: the multi-event record preserved in Loch Roag peridotite xenoliths, North Atlantic Craton

Hannah S.R. Hughes[1*], Iain McDonald[2], Matthew Loocke[2], Ian B. Butler[3], Brian G.J. Upton[3], John W. Faithfull[4]

[1]School of Geosciences, University the Witwatersrand, Private Bag 3, Wits 2050, Johannesburg, South Africa
[2]School of Earth and Ocean Sciences, Cardiff University, Main Building, Cardiff CF10 3AT
[3]School of Geosciences, University of Edinburgh, Edinburgh EH9 3JW
[4]Hunterian Museum and Art Gallery, University of Glasgow, Glasgow G12 8QQ

*Corresponding author email: hannah.hughes@wits.ac.za; Telephone: +27(0)117176547

Submission to: ***Lithos (special issue for European Mantle Workshop)***[1]

Keywords**:** SCLM, sulphide, PGE, xenolith, metasomatism

[1] **Abbreviations**: North Atlantic Craton (NAC), Great Glen Fault (GGF), North Atlantic Igneous Province (NAIP), British Palaeogene Igneous Province (BPIP), subcontinental lithospheric mantle (SCLM), platinum-group elements (PGE), highly siderophile elements (HSE), base metal sulphide (BMS)

Abstract

The role of the subcontinental lithospheric mantle as a source of precious metals for mafic magmas is contentious and, given the chalcophile (and siderophile) character of metals such as the platinum-group elements (PGE), Se, Te, Re, Cu and Au, the mobility of these metals is intimately linked with that of sulphur. Hence the nature of the host phase(s), and their age and stability in the subcontinental lithospheric mantle may be of critical importance. We investigate the sulphide mineralogy and sulphide *in situ* trace element compositions in base metal sulphides (BMS) in a suite of spinel lherzolite mantle xenoliths from northwest Scotland (Loch Roag, Isle of Lewis). This area is situated on the margin of the North Atlantic Craton which has been overprinted by a Palaeoproterozoic orogenic belt, and occurs in a region which has undergone magmatic events from the Palaeoproterozoic to the Eocene.

We identify two populations of co-existing BMS within a single spinel lherzolite xenolith (LR80) and which can also be recognised in the peridotite xenolith suite as a whole. Both populations consist of a mixture of Fe-Ni-Cu sulphide minerals, and we distinguished between these according to BMS texture, petrographic setting (i.e., location within the xenolith in terms of 'interstitial' or within feldspar-spinel symplectites, as demonstrated by X-ray Computed Microtomography) and *in situ* trace element composition. Group A BMS are coarse, metasomatic, have low concentrations of total PGE (< 40 ppm) and high $(Re/Os)_N$ (ranging 1 to 400). Group B BMS strictly occur within symplectites of spinel and feldspar, are finer-grained rounded droplets, with micron-scale PtS (cooperite), high overall total PGE concentrations (15-800 ppm) and low $(Re/Os)_N$ ranging 0.04 to 2. Group B BMS sometimes coexist with apatite, and both the Group B BMS and apatite can preserve rounded micron-scale Ca-carbonate inclusions indicative of sulphide-carbonate-phosphate immiscibility. This carbonate-phosphate metasomatic association appears to be important in forming PGE-rich sulphide liquids, although the precise mechanism for this remains obscure. As a consequence of their position within the symplectites, Group B BMS are particularly vulnerable to being incorporated in ascending

mantle-derived magmas (either by melting or physical entrainment). Based on the cross-cutting relationships of the symplectites, it is possible to infer the relative ages of each metasomatic BMS population. We tally these with major tectono-magmatic events for the North Atlantic region by making comparisons to carbonatite events recorded in crustal and mantle rocks, and we suggest that the Pt-enrichment was associated with a pre-Carboniferous carbonatite episode. This method of mantle xenolith base metal sulphide documentation may ultimately permit the temporal and spatial mapping of the chalcophile metallogenic budget of the lithospheric mantle, providing a blueprint for assessing regional metallogenic potential.

1. Introduction

Mantle xenoliths provide a direct but incomplete view of the lithospheric mantle and its history of magmatic and/or metasomatic events (e.g. Pearson *et al.,* 2003). The role of the subcontinental lithospheric mantle (SCLM) in hosting metals such as Cu, Mo, Se, Te, the platinum-group elements (PGE) and Au, has been widely discussed (cf. Mitchell and Keays 1981; Groves *et al.,* 1987; Groves & Bierlein, 2007; Arndt, 2013, and references therein). Many of these metals are strongly chalcophile and the ability of the shallow mantle to store or release them therefore largely depends on the nature and behaviour of their main hosts, Fe-Ni-Cu sulphides and platinum-group minerals (PGM) (e.g., Lorand *et al.,* 2008; 2013; Lorand & Luguet, 2016; Luguet & Reisberg, 2016), and the type of metasomatic fluid, oxidation state and sulphide-saturation of partial melts with which they interact (Aulbach *et al.,* 2016).

The composition of the lithospheric mantle in terms of PGE and other chalcophile metals has been extensively documented and studied in the context of lithospheric age, tectonic/geodynamic setting, and the presence and composition of the late veneer event (e.g., Jagoutz *et al.*, 1979; Morgan 1986; Pattou *et al.,* 1996; Alard *et al.,* 2000; Holzheid *et al.,* 2000). Studies based on bulk rock geochemistry (e.g., Maier *et al.,* 2012) may be prone to significant nugget effects because of the heterogeneous distribution of PGE-bearing microphases (Lorand *et al.,* 2013), and thus detailed investigations that combine base metal sulphide petrography, mineral trace element compositions and isotopic systematics (particularly for the Re-Os system) are vital to assess the true complexity of the upper mantle sulphur and chalcophile element reservoir (e.g., Alard *et al.,* 2000, 2005; Aulbach *et al.,* 2009; González-Jiménez *et al.,* 2014; Griffin *et al.,* 2002, 2004; Harvey *et al.,* 2010; Lorand *et al.,* 1990, 2003, 2008, 2010; Luguet *et al.,* 2003, 2004; Marchesi *et al.,* 2013; Szabo *et al.,* 1995; Wainwright *et al.*, 2015).

Advances of *in situ* analytical techniques have led to a deeper understanding of how accessory particles that comprise aggregates of Fe-Ni-Cu sulphide minerals (hereafter termed “base metal

sulphides" (BMS)) and platinum-group minerals (PGM) control the chalcophile element budget of the upper mantle (Lorand *et al.*, 2013; Lorand & Luguet, 2016 and references therein). This has led to the observation that several populations of BMS may be present in upper mantle samples. Most commonly there are: (i) rounded BMS with compositions similar to monosulphide solid solution (Mss) that can occur in intergranular positions or as inclusions in olivine and/orthopyroxene; and (ii) Cu-rich BMS that are restricted to intergranular sites. These two major populations generally have distinct PGE systematics – Mss-type BMS are Os-, Ir-, Ru- and Rh-enriched with unradiogenic Os-isotopic compositions, while Cu-Ni-rich BMS are typically Pd- (and sometimes Au-) enriched with more radiogenic Os-isotopic compositions (Burton *et al.*, 1999; Alard *et al.*, 2002, 2011; Lorand *et al.*, 2013 and references therein). Mss-type sulphides are most commonly interpreted as sulphide residual after partial melting whereas the Cu-rich BMS formed as a result of melt infiltration or metasomatism (e.g. Guo *et al.*, 1999; Alard *et al.*, 2000; Lorand & Alard, 2001; Aulbach *et al.*, 2004; Lorand & Grégoire, 2006; Powell & O'Reilly, 2007; Zheng *et al.*, 2007; Alard *et al.*, 2011; Saunders *et al.*, 2015; Luguet and Reisberg, 2016). However recent literature has increasingly documented a more complicated correspondence between textural setting and BMS trace element composition (e.g., González-Jiménez *et al.,* 2014; Wainwright *et al.,* 2015).

A study by Delpech *et al.* (2012) on Kerguelen mantle xenoliths found that interstitial BMS may be produced by melt-rock reactions during metasomatism and/or by sulphidization reactions of supercritical (S- or CO_2-rich) fluids with mantle olivine. Delpech *et al.* (2012) argued that these BMS were formed during refertilisation of harzburgitic mantle by large volumes of alkaline-silicate melts, then by small-volume volatile-rich silicate melts, and finally by small volumes of carbonate-rich fluids. The latter events were associated with a distinct generation of metasomatic BMS, and reveal complex carbonate-sulphide associations in the mantle lithosphere (Menzies & Dupuy, 1991; Grégoire *et al.*, 2000; Lorand *et al.*, 2004; Moine *et al.*, 2004). Specifically, the population of BMS formed by sulphidization reactions was selectively enriched in S, Cu, Pd, Pt and Os, and this evidence has since been used to infer the geochemical fingerprints of sulphide crystallisation from carbonate-

or CO_2-rich fluids during mantle metasomatism in an off-craton environment (Delpech *et al.*, 2012; Lorand *et al.*, 2013; Lorand & Luguet, 2016).

The complexity of the upper mantle sulphur budget reflected by multiple BMS populations is widely recognised. However, the implications of this for the supply of chalcophile elements to magmas that are either sourced from, or that traverse, the SCLM, and hence the regional implications for orthomagmatic sulphide-hosted Ni-Cu-PGE mineral deposits, are not so widely established (Griffin *et al.,* 2013). Generalised assumptions about the nature of mantle sources for chalcophile elements may be oversimplified if observed mantle lithologies and sulphide mineralogy are not taken into account. When assessing the metallogenic signature of a region, a holistic understanding of the nature and setting of refractory or fusible BMS populations in the lithospheric mantle (as recorded by mantle xenoliths), must be considered. This must include an assessment for the vulnerability of BMS to melting and remobilisation by ascending magmas, (e.g., Bedini *et al.*, 1997; Pearson *et al.*, 2003; Lorand *et al.*, 2004; Lorand & Luguet, 2016; Luguet & Reisberg, 2016; Hughes *et al.,* 2015a). This is pertinent in the prediction of the precious or critical metal characteristics of sulphide mineralisation (Hughes *et al.,* 2015a, 2016).

In this study, we present *in situ* analyses for PGE, Au, Re and semi-metals (As, Sb, Se, Te and Bi) for two distinct populations of intergranular BMS, in distinct textural settings (as supported by X-ray computed microtomography (µCT), within a single spinel lherzolite mantle xenolith from the Eocene Loch Roag monchiquite dyke in NW Scotland. We compare the *in situ* BMS-hosted element data with bulk rock major and trace lithophile element and chalcophile element data geochemistry for this and other Loch Roag spinel lherzolite xenoliths (Hughes *et al.,* 2014, 2016). The Loch Roag dyke entrained xenoliths from a fragment of the North Atlantic Craton and probably represents Archaean SCLM underlying the craton edge that was significantly re-worked in the Palaeoproterozoic and subsequently rifted during the opening of the North Atlantic in the Palaeogene.

1.1 Geological setting

Mantle xenolith localities in Scotland span five tectonic terranes (Upton *et al.,* 2011) with each terrane delineated by a major lithospheric lineament (Fig. 1a). In NW Scotland, the Archaean – Palaeoproterozoic Lewisian Gneiss Complex makes up the British portion of the North Atlantic Craton (NAC), characterised by the exposed basement of the Caledonian foreland bounded to the east by the Moine Thrust Zone (MTZ). The Lewisian Gneiss Complex comprises mid-late Archaean tonalite-trondhjemite-granodiorite (TTG) gneisses, with minor mafic-ultramafic and metasedimentary components, that have been reworked by several Late Archaean and Palaeoproterozoic tectonic events (e.g., Bridgwater *et al.*, 1973; Park & Tarny, 1987; Park, 1994; Park, 1995; Baba, 2002; Kinny *et al.*, 2005a; Park, 2005; Goodenough *et al.*, 2013).

Early Palaeoproterozoic extension (c. 2.4 Ga) led to the formation of a large igneous province (LIP), now represented by the Scourie Dyke Swarm (e.g., Davies & Heaman, 2014). The Scourie Dyke tectono-magmatic event coincided with a carbonatitic metasomatic event recognised in the Loch Roag xenocryst assemblage by model Nd-isotopic ages (c. 2.3-2.5 Ga; Long *et al.*, 1991) that may also be related to carbonatitic intrusions in the western Greenlandic NAC c. 2.6 Ga; Larsen & Rex, 1992 and references therein).

Elsewhere on the marginal cratonic portion of the Scottish lithosphere (i.e., north of the Great Glen Fault, Fig. 1a) Neoproterozoic (c. 550 Ma) carbonatitic events have been identified based on clinopyroxene Sr-Nd isotopic compositions of Streap Comlaidh and Rinibar mantle spinel lherzolite xenoliths (e.g., Bonadiman *et al.,* 2008). Metasomatic clinopyroxenes can also be identified, using *in situ* trace element geochemistry, in the Loch Roag spinel lherzolites (Hughes *et al.,* 2015b), corroborating the inferred carbonatite-related metasomatism by Long *et al.* (1991). Hence it is suggested that multiple carbonatitic metasomatic events, ranging in age from the early Proterozoic to the late Neoproterozoic, are recorded by the Scottish marginal cratonic SCLM and these events are broadly correlated with carbonatite and kimberlite intrusions in the Greenlandic NAC (Larsen & Rex, 1992).

In the Palaeogene, the North Atlantic Igneous Province (NAIP) formed by the impingement of the proto-Icelandic mantle plume beneath cratonic lithosphere. This rifted the NAC such that the Lewisian Gneiss Complex became separated from Greenland during the opening of the North Atlantic c. 62 Ma (Saunders *et al.*, 1997).

1.2 Loch Roag monchiquite dyke – host to the xenolith suite

The 70cm wide Loch Roag monchiquite dyke (a mafic lamprophyre with brown amphibole, Ti-augite, olivine and biotite; see Gillespie and Styles, 1999) is host to the mantle xenoliths in this study and sits on the leading edge of the rifted NAC (Fig. 1b). It is mid-Eocene in age (^{40}Ar-^{39}Ar mica age, 45.2 ± 0.2 Ma; Faithfull *et al.*, 2012) and thus the youngest known magmatic event in the UK. Whilst most mantle xenolith-bearing dykes in western Europe south of Scandinavia pass through lithosphere that has experienced Phanerozoic (Caledonian/Hercynian/Alpine) orogenesis, the lithosphere traversed by the Loch Roag dyke has remained undeformed since the Mesoproterozoic (c.f., 1.6 Ga Laxfordian event). Hence this dyke contains a suite of upper mantle and crustal xenoliths and xenocrysts, unusual in comparison to elsewhere in the wider UK and Europe (Upton *et al.*, 1983). It comprises a diverse range of lithologies and megacrysts including spinel lherzolites, glimmerites, anorthosites/anorthoclasites, gabbros and syenite xenoliths, phlogopite 'books', apatite and corundum xenocrysts (Upton *et al.*, 1983; Hunter & Upton, 1987; Menzies *et al.*, 1987; Menzies & Halliday, 1988; Long *et al.*, 1991; Upton *et al.*, 1999; Upton *et al.*, 2011).

1.3 Petrography and bulk geochemistry of the Loch Roag spinel lherzolite xenoliths

Detailed studies of the non-sulphide mineralogy, mineral chemistry, bulk rock geochemistry and isotopic compositions of the Loch Roag xenoliths have previously been documented by Hunter & Upton (1987), Menzies *et al.* (1986) and Upton *et al.* (2011), and recently revisited by Hughes *et al.* (2015b, 2016). Here we summarise these studies to provide relevant information for

characterisation of the sulphide mineralogy and chemistry, and identification of different BMS populations.

The spinel lherzolite xenoliths are typically up to 4 cm in diameter, slightly rounded, and have an oxidised green-orange-brown 'rim' (normally up to 1 cm thick) at the contact with the host dyke (Fig. 2a). Haematite and sulphate minerals (such as barite) are common in these halos and are ascribed to reaction of the peridotite with the host magma (e.g., Fig. 2a). However, the central portions of the xenoliths comprise grey peridotite unaffected by reaction with the host dyke. These cores have sub-equigranular, granoblastic and porphyroblastic textures with crystal sizes typically ranging 1 to 2 mm with rare orthopyroxene porphyroclasts up to 10 mm in length. Because of their small size, very few of the xenoliths have unaltered peridotite interiors sufficiently large for effective sampling – thus two larger xenoliths 'LR80' and 'LR81' appear frequently in the literature as these offer the best opportunity for extensive and repeated sampling and analysis (both for bulk rock and *in situ* techniques). These xenoliths were sliced into a series of 5-10 mm wide sections and this curated material has been the focus of several studies since the 1980's and this current work.

Olivine compositions in spinel lherzolite xenoliths LR80 and LR81 are $Fo_{89.8\text{-}88.7}$, with 0.3-0.4 wt.% NiO (Hunter and Upton, 1987). Clinopyroxenes are systematically SiO_2-richer but Al_2O_3-poorer compared to other Scottish lherzolite xenoliths (i.e., 54 wt.% vs. 51-52 wt.% SiO_2 and 4.2-4.7 wt.% vs. 5-8 wt.% Al_2O_3 respectively; Upton *et al.*, 2011). Mean orthopyroxene compositions are approximately $En_{89}Fs_{10}Wo_1$ and these are relatively Al-poor in comparison to other Scottish lherzolites (2.2-2.6 wt.% vs. 2.0-5.3 wt.% Al_2O_3 respectively; Upton *et al.*, 2011).

Spinel grains appear 'corroded' and are surrounded by, and intergrown with, sodic-feldspars forming symplectite-like pockets (Fig. 2b-c) along spinel-clinopyroxene, clinopyroxene-olivine and olivine-olivine grain boundaries (Hunter & Upton, 1987; Upton *et al.*, 2011). Feldspars are anorthoclase-oligoclase with a mean composition of $Or_{7.6}Ab_{80.8}An_{11.6}$ (Hunter & Upton, 1987; Upton *et al.*, 2011). Spinel has 35-49 wt.% Cr_2O_3 (notably higher than other Scottish xenoliths which typically have < 20

wt.%; Upton *et al.,* 2011) and in rare cases, very fine granular high-Cr spinel (lacking Mg and Al) can be found as atoll-like features in the symplectites and nucleating on the edge of the larger corroded Al- and Mg-bearing (hercynitic) spinel (Fig. 2c). All spinel and feldspar occur within these 'symplectites'. In some cases, micrometric intergrowths of sodic-feldspar with Na-rich clinopyroxene and olivine form a zone up to 250 µm wide surrounding the spinel-feldspar symplectites. In rare cases (typically areas on the outer margins of the xenoliths) melt percolation recorded as finely crystalline ilmenite-chromite-plagioclase-biotite patches follow the path of the symplectites.

Bulk geochemistry of the Loch Roag lherzolites was first published by Menzies *et al.* (1986), but the xenoliths have subsequently been resampled and reanalysed by Hughes *et al.* (2014, 2015b, 2016) – a summary of which can be found in Table 1. Because of the limited material available, most powdered xenolith samples included some proportion of the outer reaction rim described above, however in the case of sample LR80 (labelled on Fig. 3), the xenolith was large enough that this reaction rim could be entirely removed prior to powdering. A second slice of unaltered LR80 material was kept for *in situ* mineral analysis for the purposes of this study.

Anhydrous bulk rock Cr/Al, Al/Si and Ca/Si ratios for Loch Roag lherzolites (Hughes *et al.*, 2015b) are compared with harzburgites, lherzolites and wehrlites from west Greenland in Figures 3a and 3b. The latter have low Al/Si and Ca/Si and extremely variable Cr/Al (Wittig *et al.,* 2010) relative to 'Primitive Upper Mantle' (PUM; McDonough & Sun, 1995). The Loch Roag lherzolites form an intermediate group between Greenlandic and PUM compositions and the elevated Ca/Si and Al/Si of Loch Roag suggests significant refertilisation. Comparing anhydrous Cu vs. Cr/Al highlights a significant enrichment in Cu for all Loch Roag lherzolites (particularly unaltered LR80) in comparison to both Greenlandic mantle xenoliths and PUM. This probably reflects the higher overall abundance of BMS present in the Loch Roag xenoliths, rather than specifically a higher chalcopyrite component, as bulk rock Cu concentration will more faithfully record sulphide abundance than Ni or Fe (for which the bulk signal will be swamped by olivine and to a lesser extent pyroxene).

Upton *et al.* (2011) used a simple melting model for Al and Mg in ortho- and clinopyroxene to demonstrate that most Scottish spinel lherzolite xenoliths (including Loch Roag) have orthopyroxene compositions consistent with being residual after melt extraction. In contrast, the melting curve calculated for clinopyroxene does not fit the compositions in Loch Roag xenoliths (and most other Scottish xenolith suites) and therefore the clinopyroxenes cannot be residual. In addition, following studies into the relative abundances of Zr-Hf in pyroxenes as an indicator of cryptic metasomatism (Downes *et al.,* 2015), the high Zr/Hf ratios of the Loch Roag clinopyroxenes have been interpreted to indicate cryptic metasomatism of the spinel lherzolites (Hughes *et al.,* 2015b).

2. Analytical techniques and methodology

2.1 Petrography and mineral chemistry analysis

Petrographic studies on polished thin sections and polished blocks were employed to identify xenolith textures. Further examination, mapping and quantitative microanalysis was carried out on a Cambridge Instruments S360 scanning election microscope (SEM) at Cardiff University. Quantitative microanalyses were obtained using an Oxford Instruments INCA Energy EDS analyser attached to the SEM, with operating conditions set at 20kV and specimen calibration current of ~2 nA at a fixed working distance of 25 mm. Analytical drift checks were carried out every 2 hours using the Co reference standard and a comprehensive suite of standards from MicroAnalysis Consultants Ltd were used to calibrate the EDS analyser. All Loch Roag SEM quantitative major element data (Fe, Ni, Cu, S) for individual sulphide minerals are in Supplementary Table A and a representative selection of these data are presented in Table 2.

Polished blocks were selected for laser ablation inductively coupled plasma mass spectrometry (LA-ICP-MS) for sulphide trace element analysis. Time resolved analysis (TRA) by LA-ICP-MS was performed on BMS aggregates containing multiple sulphide minerals at Cardiff University on a New

Wave Research UP213 UV laser system attached to a Thermo X Series 2 ICP-MS. Both line and spot analysis were used, depending on the size of the BMS, and independently calibrated. For lines, a minimum length of ~80 µm and a beam diameter of 15 µm was used, with laser operating conditions of 10 Hz frequency, 0.063 mJ at 4.98 Jcm^{-2} and sample translation at 6 µm sec^{-1}. For spot analysis, beam size was 40 µm and the same laser operating conditions as for the line analyses were employed. BMS < 80 µm diameter were only analysed by spot analysis. Acquisition times ranged 40 to 180s with a gas blank measured for 30s prior to laser ablation. Major element abundances (Fe, Ni, Cu, S) of the sulphide were measured by SEM prior to LA-ICP-MS, and a weighted mean of ^{33}S (taking into account the % of each end-member sulphide present in each BMS grain, per BMS analysed by LA-ICP-MS) was used as an internal standard for trace element calibration. Gas blank subtraction and internal standard corrections were carried out on Thermo Plasmalab software.

Synthetic Ni-Fe-S quenched sulphide standards were used for LA-ICP-MS calibration, including S, Ni, Fe and Cu as major elements, and Co, Zn, As, Se, Ru, Rh, Pd, Ag, Cd, Sb, Te, Re, Os, Ir, Pt, Au and Bi as trace elements. The compositions and details of analytical methods for these standards are presented in Prichard *et al.* (2013) and further procedural details are available in Smith *et al.* (2014). Standards 1, 2 and 3 were used for calibration of Fe, Ni, Cu, Co and Zn, as well as matrix-matched corrections for argide species, which interfere with light PGE isotopes ($^{59}Co^{40}Ar$, $^{61}Ni^{40}Ar$, $^{63}Cu^{40}Ar$, $^{65}Cu^{40}Ar$ and $^{66}Zn^{40}Ar$). Standard 1 was used in corrections for ^{106}Cd on ^{106}Pd and ^{108}Cd on ^{108}Pd. Argide and isobaric-corrected standard data are presented in Supplementary Table B, for Ru, Rh and Pd. Independent corrections for isotopes of the same element (e.g., $^{66}Zn^{40}Ar$ and ^{106}Cd on ^{106}Pd, and ^{108}Cd on ^{108}Pd) showed < 20% (commonly < 5%) variance, indicating that the correction criteria are appropriate. The accuracy for PGE and Au was checked by analysis of the Laflamme-Po724 standard as an unknown against the Cardiff quenched sulphide standards (results in Supplementary Material Table B). The small size of many sulphides prevented repeat analyses and therefore 1σ precision based on TRA counting statistics are typically 2-16% (concentrations 10-100 ppm), 10-27% (1-10 ppm) and 23-80% (< 1 ppm). A representative selection of TRA for BMS analysed are presented in

the Supplementary Material and all Loch Roag LA-ICP-MS sulphide data are reported in Supplementary Table C. A representative selection of these data are presented in Table 3.

2.2 Element maps – estimations of the modal abundance of sulphide

Whole thin-section element maps of the samples were collected on a Zeiss Sigma HD analytical SEM outfitted with dual 150 mm^2 active area EDS detectors at Cardiff University. This used a 20 µm step-size (400 μm^2 per pixel) and a pixel dwell time of 15 ms in order to create effective phase maps for pyroxenes, olivine, spinel, feldspars, sulphides, carbonates and phosphates (see Supplementary Material for all images and maps – PNG files named 'LR80-' accordingly). These maps have previously been published in Hughes *et al.* (2016).

The modal abundance of BMS (counted as total sulphide without differentiating between Ni, Fe or Cu end-member compositions) per thin section of LR80 was estimated in each case using the built-in PhaseMap tool in Oxford Instruments Aztec Energy software, which accounts for the shape of the BMS within each thin section. The modal abundances of BMS, along with other accessory and modally-major minerals for each scanned thin section are provided in Table 4 (note that section numbers correspond to those of the phase maps presented in the Supplementary Material).

2.3 X-ray Computed Microtomography (µCT)

X-ray computed microtomography (µCT) provides a non-destructive technique by which to establish and visualise the internal characteristics of mantle xenoliths. This is particularly effective for rare samples whereby preservation of material may be paramount for curation. µCT scanning for geoscience applications was developed by Carlson *et al.* (2000) and Ketcham & Carlson (2001). It has been further advanced to visualise sulphide minerals (e.g., Kyle & Ketcham, 2003; Kyle *et al.*, 2004; Godel *et al.*, 2006; Godel *et al.*, 2013), and has been applied to meteorites (e.g., Kondo *et al.*, 1997), diamondiferous eclogitic xenoliths (e.g., Schulze *et al.*, 1996; Richardson *et al.*, 2014; Howarth *et al.*,

2015) and diamonds (Jacob *et al.*, 2011; Agrosi *et al.*, 2016). The details surrounding µCT scanning are given in Denison *et al.* (1997), Ketcham & Carlson (2001) and Mees *et al.* (2003).

Tomographic data from a slice and a 5mm diameter sub-core of LR80 were acquired using a µCT instrument designed and built at the University of Edinburgh. The instrument comprised a 10-160 kV Feinfocus transmission X-ray source, a MICOS UPR-160-Air rotary table and a Perkin Elmer XRD0822 1 megapixel flat panel amorphous silicon detector with a Gd2O2S:Tb scintillator, operated by control software developed in-house. In total 2000 projections, each the average of two exposures of two seconds, were collected through a 360° sample rotation, using radiation generated at a peak energy of 80 kV and 2.8 W target power. Tomographic slices were reconstructed by filtered back projection using Octopus 8.7 (Vlassenbroek *et al.*, 2010) and visualised in 2D and 3D using Fiji and Avizo 9 software.

3. Results

3.1 BMS petrography

One sample (LR80) was large enough (approximately 6 cm diameter of 'unaltered' core) to be cut into slices, subsequently sampled by 8 thin sections and polished blocks, and petrographically mapped (e.g., Fig. 2 and supplementary material whole section scans). Thus, LR80 provided a rare opportunity to document the locations and petrography of BMS, including relationships between different sulphide minerals, using SEM backscattered electron (BSE) imaging. One thin section from a second xenolith, LR90, contained additional BMS within a symplectite pocket (see below) and these were also studied. BMS were classified according to size, location, relationships with surrounding non-sulphide minerals, BMS texture (relationship between constituent sulphide minerals making up each BMS grain, with reference made to textural descriptions and classifications first defined by

Lorand & Conquéré, 1983; Dromgoole & Pasteris, 1987; Szabo & Bodnar, 1995 and Guo *et al.*, 1999) and compositions.

All BMS occur as intergranular components in the Loch Roag peridotites and no wholly enclosed BMS inclusions were found. Using the classification criteria outlined above, two principal BMS groups can be distinguished (see Table5). Group A BMS represent ~70% of the BMS grains observed and/or analysed. They are coarse (generally 50-500 µm) and interstitial to olivine or pyroxene (Fig. 4a), often occurring at protogranular triple junctions (e.g., Fig. 4b), and without any systematic association with a specific modal mineral. EDS element mapping across three thin sections of xenolith LR80 (see Supplementary Material) shows no enrichment in Ca, Na or P around these BMS (c.f. the Group B BMS below). Detailed BSE images of Group A BMS reveal internal textures (Fig. 5) with flame-like intergrowths of pyrrhotite and pentlandite (that resemble those formed by high temperature sulphide exsolution of Mss; Lorand & Luguet, 2016), and massive, granular pentlandite and cross-hatched zones of chalcopyrite. The proportion of chalcopyrite within a single BMS grain can be quite variable among the Group A BMS (cf. Fig. 5a-b, c) ranging from 0% to 14% (see Table 5).

By contrast, Group B BMS (~30% of the total number of BMS grains) are systematically associated with the abundant spinel-feldspar symplectites in LR80 (Fig. 4c) and also in symplectite pockets in LR90. Group B BMS typically appear as droplet-like features, generally < 100 µm, enclosed within the feldspar component of symplectites (which surround the skeletal spinel component of symplectites; Fig. 6a-b, or rarely occur within feldspar that feeds into micrometric intergrowths with Na-rich clinopyroxene and olivine forming a zone up to 250 µm wide surrounding the spinel-feldspar symplectites, Fig. 6d). Proportions of the major sulphide minerals in Group B BMS are summarised in Table 5. In some cases cooperite (Pt-sulphide) has exsolved from BMS and formed a discrete platinum-group mineral (PGM) phase, often associated with chalcopyrite (Fig. 6c-d). These PGM (up to 3 µm long) are only observed in group B BMS. Sometimes Group B BMS have a spongy appearance because of their incorporation of numerous non-sulphide inclusions (serpentinite and

$CaCO_3$ < 30 µm; Fig. 6e-f). Serpentine-filled inclusions are generally polygonal, whilst $CaCO_3$ inclusions are rounded. These spongy BMS are also < 100 µm in diameter and closely resemble the droplet-like appearance of their inclusion-free counterparts, although the former tend to have a lower modal abundance of chalcopyrite (2% for inclusion-bearing BMS vs. 8% for inclusion-free Group B BMS). Whether this is a real enrichment in Cu or a sampling bias induced by the small number of inclusion-bearing BMS and the random nature of sectioning is unclear.

A discontinuous vein of apatite runs through xenolith LR80 and also contains BMS (Fig. 7a). Apatite crystals are 50-200 µm in size, irregularly shaped and typically associated with $CaCO_3$ and feldspar identical in composition to that of the symplectite pockets. Droplet-like BMS up to 150 µm diameter (occasionally with apatite inclusions < 10µm diameter) occur within this vein (Fig. 7b). These BMS can have $CaCO_3$ inclusions and have similar sizes, shapes and mineral textures to the other Group B BMS. Apatites display fine spongy textures with abundant inclusions of $CaCO_3$ (typically < 5µm, and can be < 1µm) and less common sub-micron-scale Ni-Fe sulphide inclusions (Fig. 7c). This produces an unusual immiscibility texture between phosphate, carbonate and sulphide. Very fine skeletal apatite crystals (up to 5 µm long) also occur in the feldspar of the vein surrounding the spongy larger apatite crystals (Fig. 7c).

3.2 Xenolith three-dimensional textures and structures - µCT

We have used µCT to investigate the degree of interconnectivity of the spinel-feldspar symplectites throughout LR80, to establish the pathways available to sulphide liquids, and the relationships between the two BMS populations. Figure 8 shows an example of a 2D slice of the µCT data (Fig. 8a) and 3D reconstruction µCT freeze-frames (Fig. 8b-e) generated from the same polished blocks of LR80 used for petrographic studies. In Figures 8b-c we have highlighted spinel (as a tracer for the symplectite portion) within a polished block approximately 3 cm diameter, by digitally removing the highest density phase (BMS) and gradually stripping the lower density silicates from the view. The accompanying supplementary material contains a video of this process. The three dimensional

distribution of spinel defines a distinct fabric within the xenolith (Fig. 8c) indicating that the xenolith is slightly sheared, which was not apparent prior to X-ray µCT scanning.

Following further processing of the µCT data, we have highlighted both the spinels and the lowest density minerals in the xenolith – serpentine (which is of low modal abundance), and feldspar within the symplectites. Figure 8d shows a sub-region of a µCT scan with spinel highlighted in blue. This smaller scale shows internal networks of symplectites within the xenolith. Displaying the low-density feldspars as a coloured semi-transparent shell shows the interconnectivity of the spinel-feldspar symplectites (Fig. 8e). µCT volumes were segmented using a global threshold to separate high density minerals (spinel and BMS) from low density minerals (feldspar in the symplectites). Using this method, partial overlap between spinel and BMS phases was unavoidable, but separation of symplectitic feldspar from these phases was reliable. For visualisation, the separated binarised volumes of the spinel and BMS are presented as volume renderings. The feldspars in the symplectites were further classified using the “label" algorithm in Avizo to identify voxels in contact with each other (by either a face, edge or vertex) so that they are labelled with a discrete colour to demonstrate connectivity through the volume. The symplectites were then converted to a surface mesh and visualised as semi-transparent structures to illustrate their relationship to spinel and BMS. This demonstrates that the spinel-feldspar symplectites form an open system through the xenolith and hence preserve a fossil network of open pathways for fluid/melt migration in the lithospheric mantle.

3.3 BMS geochemistry

Quantitative SEM (with EDS measurements) are compiled in Table 2 and LA-ICP-MS data have been compiled in Table 3 (the latter representing 75 *in situ* analyses of BMS grains in LR80 along with 8 analyses from a spinel lherzolite xenolith LR90, which is texturally and mineralogically similar to LR80). The major sulphide mineral or mixture of sulphide minerals ablated in each analysis are given in Table 3. Data are presented in Figures 9-11 and were classified according to the BMS petrography

(as outlined in Section 3.1) and their trace element compositions determined by LA-ICP-MS. Hence Figures 9-11 refer to groups A and B BMS.

None of the laser data comprise 100% single sulphide minerals, but a small subset of the data produce analyses with Fe, Ni and Cu concentrations within 96% of end-member chalcopyrite and within 95% of end-member pyrrhotite (Ni-poor Mss). One Group A analysis has 98% of the Ni expected for end-member pentlandite and two Group B analyses have Ni corresponding to 87-89% of end-member pentlandite (both termed hereafter pentlandite-88). The remainder are more complex mixtures. Mixed laser analyses from both BMS groups overlap according to metal/S, Fe/(Fe+Ni+Cu) and Ni/(Ni+Cu+Fe) ratios (Fig. 9a-c). The larger grain size of Group A BMS allowed specific analyses of coarse chalcopyrite and more chalcopyrite-rich mixtures, which led to a wide range of Cu/(Cu+Ni+Fe) ratios (0 to 0.52) compared to Group B (0 to 0.11). But this is a sampling bias controlled by sulphide mineral size and there is substantial overlap in the Cu abundance of both groups (Table 5) with no trend defined by the major element data (Table 2). However when Cu (from the LA-ICP-MS dataset) is plotted against total PGE (Os+Ir+Ru+Rh+Pt+Pd), the two BMS groups are clearly separated. Furthermore there is no correlation between Cu concentration vs PGE concentration (Fig. 9d) despite the overlap in Cu concentrations. 90% of the Group A BMS have total PGE < 10 ppm and 22% of Group A BMS have total PGE concentrations < 1ppm. Group B BMS always have > 15 ppm total PGE and there is no systematic relationship between total PGE and Cu for either BMS group.

Laser analyses with near end-member compositions are plotted on chondrite-normalised multi-element diagrams in Figure 10a. Chalcopyrite is only available for Group A and is characterised by very low concentrations of all PGE and Au. There are clear differences between the PGE, Re and Au compositions of Ni-poor Mss and pentlandite in Group A and Group B. In Group A, Ni-poor Mss and pentlandite both contain very low concentrations of Ir-group PGE (IPGE) and Rh (Fig. 10a). The Group A pentlandite analysis shows enrichment in Pt and Pd compared to the Ni-poor Mss ($(Pd/Ir)_N$ =

21.7 and 0.82 respectively). For Group B, PGE concentrations in both major sulphides are higher than their equivalents in Group A. Analyses of Ni-poor Mss and pentlandite-88 (both Group B) produce flat normalised profiles (> 10 x chondrite) from Os to Rh. The Ni-poor Mss displays a strong depletion in Pt and Pd compared with the pentlandite-88 which is enriched in Pd, with a variable negative Pt anomaly (Fig. 10a).

Collective spidergram plots for all Group A and all Group B BMS are shown in Figures 10b and 10c, respectively. It is clear that many of the features in the mixed patterns reflect varying proportions of the individual end-member component sulphide minerals. An exception to this generalisation is that normalised patterns for Group B sulphides show both positive and negative Pt anomalies ($(Pt/Ir)_N$ 0.02-11.3 and $(Pt/Pd)_N$ 0.10-442). Negative anomalies are linked with pentlandite (Fig. 10a) but strong positive anomalies are not observed in any of the sulphide end-members. Time resolved spectra (TRA) from LA-ICP-MS analyses with positive Pt anomalies (see supplementary material for examples) show extreme spikes in Pt abundance along the laser line that are integrated into the combined signal. These therefore corroborate instances where micro-particles of cooperite (PtS) have been observed in the SEM images (e.g., Fig. 6c-d) and have subsequently been sampled by the laser. Conversely, the absence of visual PGM, and the complete lack of strong positive Pt anomalies in all Group A analyses by LA-ICP-MS, suggest that cooperite or any other PGM are entirely absent from this BMS population.

On a plot of $(Pd/Ir)_N$ vs. $(Os/Ir)_N$ (Fig. 11a) Group B BMS display almost three orders of magnitude variation in $(Pd/Ir)_N$ (0.02-11.5) along a restricted range of $(Os/Ir)_N$ (0.84-1.54). Group A BMS extend this vertical $(Pd/Ir)_N$ array upwards but also scatter either side of it ($(Os/Ir)_N$ 0.18-8.7). Delpech *et al.* (2012) observed a similar vertical array in Kerguelen peridotites but with consistent scatter only to $(Os/Ir)_N$ greater than 1. The low $(Os/Ir)_N$ found in part of the Group A dataset was not found at Kerguelen.

$(Re/Os)_N$ values are > 1 in all Group A end-member sulphides and < 1 in the Group B Ni-poor Mss and pentlandite-88 (Fig. 10a). This is reflected in the mixtures where 47 out of the 52 mixed Group A analyses have $(Re/Os)_N$ values > 1 (Group A range = 0.82-188) whereas 17 out of the 23 Group B mixed analyses have $(Re/Os)_N$ < 1 (Group B range = 0.01-1.37). $(Re/Os)_N$ is not affected by the Cu content of the BMS with the groups clearly separated at equivalent Cu concentrations (Fig. 11b).

Group A and B BMS overlap in terms of S/Se ratios but the range for Group B (S/Se = 1950-3440) clusters more tightly around the primitive mantle value of 3300 (Sun and McDonough 1995) whereas Group A has a much wider range (S/Se = 1960-5680). When S/Se is plotted versus Te (Fig. 11c) it is clear that Groups A and B follow different trends. Group A BMS can be both S-rich and Te-poor compared with Group B. Tellurium concentrations for both groups are anti-correlated with Cu and the trend of Te enrichment in very Cu-rich BMS observed by Delpech *et al.* (2012) is not found in either BMS group at Loch Roag (Fig. 11d).

4. Discussion

The position of the Lewisian Gneiss Complex on the rifted edge of the North Atlantic Craton and the multiple orogenic events recorded in this region led Hughes *et al.* (2015b) to suggest that the Lewisian Gneiss Complex has long been the margin of the craton itself. This means that it is particularly vulnerable to metasomatism and refertilisation during orogenic events, unlike the central keel portions of the craton which are characteristically depleted (e.g., Pearson *et al.* 2003; Wittig *et al.*, 2010). This is illustrated in Figure 3 where the Loch Roag peridotites are enriched in Ca, Al and notably Cu, compared to the West Greenland mantle. Thus, Loch Roag xenoliths cannot be regarded as truly 'cratonic', rather as 'marginal cratonic' at best. This provides an opportunity to assess the metallogenic metasomatic and refertilisation history of this marginally cratonic SCLM as recorded by mantle BMS populations.

4.1 Multiple populations of metasomatic BMS

We have established, on the basis of petrographic setting (Table 5) and trace element geochemistry, that two discrete populations of BMS are present in the Loch Roag peridotites, and specifically that these co-exist within a single xenolith. Both groups of BMS show sulphide mineral textures similar to those formed by high temperature exsolution of Mss (monosulphide solid solution) and Iss (intermediate solid solution) through progressive cooling and subsequent sub-solidus re-equilibration, and very similar textures have been widely identified in other mantle BMS (Alard *et al.*, 2000, 2011; Aulbach *et al.*, 2004; Lorand & Grégoire, 2006; Luguet and Reisberg; 2016). The isolated nature and the absence of symplectite zones around Group A BMS, coupled with significant overlap in the major element compositions of both groups (reflected by Fe/(Fe+Ni+Cu) and Ni/(Fe+Ni+Cu) ratios; Fig. 9 and Tables 2 and 5), precludes the possibility that one group reflects the partial melting and mobilisation of the other. During incongruent partial melting of BMS, the Cu-rich portion would be mobilised first as the lowest temperature sulphide, thus leaving a Fe(Ni)-rich residue and forming a Cu-Ni-rich liquid (Holwell & McDonald, 2010; Lorand & Luguet, 2016 and references therein). If Group B BMS formed from partial melting of Group A, Group B BMS ought to be systematically Cu-rich and vice versa. This is not evident in our analyses.

As demonstrated in Figure 10, Group A and Group B end-member minerals and mixed BMS analyses have notably different PGE concentrations. Whilst subtleties in the PGE patterns for each analysis may be noted for Cu- or Ni-rich mixtures in each group, this fundamental PGE-rich vs PGE-poor categorisation is robust irrespective of the proportions of individual sulphide minerals incorporated into each BMS analysis. The trace element chemistries of Group A (e.g., $(Re/Os)_N > 1$, low IPGE, $(Pt/Ir)_N > 1$, $(Pd/Ir)_N > 1$) and Group B (e.g., $(Re/Os)_N < 1$, high IPGE and variable $(Pt/Ir)_N$ and $(Pd/Ir)_N$) have also been observed before and respectively conform to the Type 2 and Type 1 BMS of Alard *et al.* (2000). Thus, the PGE signatures for Loch Roag Group A closely resemble Cu-enriched BMS formed by melt infiltration or metasomatism while the PGE signatures of Group B could be interpreted as BMS formed from the residue of partial melting (e.g. Guo *et al.*, 1999; Alard *et al.*,

2000; Lorand & Alard, 2001; Aulbach *et al.*, 2004; Lorand & Grégoire, 2006; Powell & O'Reilly, 2007; Zheng *et al.*, 2007; Alard *et al.*, 2011; Saunders *et al.*, 2015; Luguet and Reisberg, 2016).

Group A BMS only occur between olivine crystals or at olivine-pyroxene junctions, and never as inclusions inside the major silicate minerals. These textural associations are consistent with an origin by melt infiltration or metasomatism inferred from the IPGE-poor and PPGE- and Re-rich geochemistry outlined above. However Group A BMS lack the systematic enrichment in Os over the other IPGE (reflected by both $(Os/Ir)_N$ >1), and consistently lack the low Se concentrations (< 100 ppm), high S/Se (> 3500 up to 10000) and coupled enrichment in Te and Pd that have been suggested to characterise very volatile-rich metasomatism and vapour transport of Os, Pd, Au, Re and S (e.g., Alard *et al.*, 2011; Delpech *et al.*, 2012). The textural appearance of the sulphide minerals forming Group A BMS (in addition to their interstitial setting; Table 5) would indicate a metasomatic origin (e.g., Lorand & Luguet, 2016; Aulbach *et al.,* 2016). These superficially look to be akin to 'Type-2' BMS documented in Alard *et al.* (2000), but the absence of systematic and coupled enrichment in Os, S and Pd for Group A BMS suggests that these are compositionally unlike such BMS proposed to have formed by vapour transport processes (e.g., Alard *et al.*, 2011; Delpech *et al.*, 2012) and therefore a different metasomatic agent may be envisaged, with high S-content at sulphide saturation (e.g., Aulbach *et al.,* 2016).

The real paradox at Loch Roag is the origin of the Group B BMS that co-exist with Group A BMS within each spinel lherzolite xenolith and are common in samples from at least two xenoliths (samples LR80 and LR90, which were extensively documented in this study). While their trace element signatures superficially resemble residual BMS, Group B are always found in spinel-feldspar symplectites. Detailed petrographic studies and μCT scans clearly demonstrate that the spinel-feldspar symplectites form an interconnected network throughout the xenolith (Fig. 8d-e). Further, the composition of the feldspar in these symplectites (the only feldspar in Loch Roag spinel lherzolite xenoliths) is Na-rich ($Or_{7.6}Ab_{80.8}An_{11.6}$; Hunter & Upton, 1987; Upton *et al.*, 2011) and thus cannot be

related to break-down of spinel during decompression (Rampone *et al.*, 1993; Upton *et al.*, 2011). This suggests that the symplectite feldspar was formed by influx of Na-rich melt or fluid. Whether this influx made use of pre-existing pathways through the mantle remains unclear but, given the skeletal texture of spinel (that may be crystallographically controlled e.g., Figs. 2, 4c-d, 6) and its intergrowth with feldspar, it is possible that partial decompression of spinel to plagioclase may have preceded this melt influx, weakening the peridotite and providing a network along which the Na-rich melt or fluid could permeate. Further, the low Al_2O_3 content of orthopyroxene in the Loch Roag peridotite xenoliths may record destabilisation of garnet during rifting pre-entrainment of the xenoliths. Additionally, some Group B BMS have apatite and carbonate inclusions (e.g. Fig. 6e-f; Table 5) and/or are spatially associated with 'spongy' apatite crystals (themselves with carbonate and sulphide inclusions; Fig. 7). This unequivocally demonstrates that the Na-rich melt or fluid responsible for feldspar formation in the symplectites was rich in CO_2, P and S and thus we envisage a three-way immiscibility associated with this event.

Given the exclusive association of Group B BMS with the symplectites (Fig. 4c-d and Fig. 6a-b) and the cross-cutting nature of these symplectite networks (Fig. 8e), it is clear that Group B BMS developed *after* the formation of Group A BMS. Hence the paradoxical dilemma: Group A BMS (relatively old) in many ways resemble metasomatic sulphides, yet Group B BMS (relatively young) are geochemically most akin to residual IPGE-enriched BMS (e.g. Alard *et al.*, 2000; Lorand & Luguet, 2016 and references therein). Further, the shapes and textural associations observed with Group B BMS demonstrate that they formed as immiscible droplets in an environment enriched in carbonate, phosphate and lithophile elements. The exact mechanism for this remains unclear at this stage. Nevertheless, despite the apparently similar geochemistry, the Group B sulphides at Loch Roag cannot be residual BMS (Type 1 BMS of Alard *et al.*, 2000).

Further support for a non-residual origin for Group B comes from the presence of Pt-sulphide (cooperite) in Group B BMS, which implies a high sulphur fugacity (fS_2) - but not so high fS_2 as to lead

to formation of pyrite, which is not observed in the Loch Roag BMS populations. More typically in mantle lithologies, Pt is found in Pt-Ir-Os alloys and these are interpreted to have formed by desulphidation of Mss (as demonstrated in the experimental work of Peregoedova *et al.*, 2004 and observed by Fonseca *et al.*, 2012). The partition coefficient of Pt (D_{Pt}) decreases with decreasing fS_2 from S-oversaturated (pyrrhotite-rich) to S-undersaturated (Fe metal-rich) conditions (Mungall *et al.*, 2005) and thus leads to PGE alloy nucleation. During incongruent partial melting of mantle BMS (forming an initial Cu-Ni-rich sulphide liquid and a residue of Fe-Ni-rich Mss), very high PGE tenors will be achieved in the residue due to high overall D_{PGE}, leading to saturation for Pt-Ir alloys by just 10% partial melting (Mungall & Brenan, 2014). No PGE alloys have been found in the Loch Roag xenoliths, in either BMS group. The prevalence of Pt-sulphide in Group B BMS, strictly hosted in the spinel-feldspar symplectites, therefore cannot be explained by partial melting of BMS and remobilisation of sulphides within this lithology (i.e., closed-system behaviour) and, in accordance with inferences already made above, suggests that Group B BMS were introduced during a Na-rich metasomatic event that postdates formation of the Group A BMS.

A log fS_2 – T diagram was constructed from experimental and calculated stabilities of PGM in Lorand & Luguet (2016) and this indicates that very specific fS_2 and temperature conditions are required to form Pt-sulphides in mantle lithologies. For temperatures ranging 900 to 1150^{o}C along the olivine-orthopyroxene-Mss curve (from Eggler & Lorand, 1993) fS_2 ranges from 0.01 to 0.10. The position of Pt-sulphide in Group B BMS (within chalcopyrite and/or at the edge of the BMS grains; Fig. 6c-d) suggests they exsolved during cooling and fractionation of the sulphide droplets. Arsenic, Te, Bi and Sb levels are systematically low in both BMS groups (Table 3) indicating that semi-metals were present at insufficient concentrations to scavenge Pt (or PGE in general) into a late-stage semi-metal-rich immiscible liquid (e.g., enriched in Te, Bi, As and Sb) to exsolve as Pt-Bi-Te-Sb-As PGM (Helmy *et al.,* 2007; Holwell and McDonald 2010). The absence of Te-bearing microphases and the lack of any correlation between Te and elevated Cu or Pd concentrations (c.f. Delpech *et al.*, 2012) further confirm the Te-poor nature of all Loch Roag BMS.

Tellurium and gold in Loch Roag BMS

The cause for the low Te in all Loch Roag BMS also remains unclear. Whilst Se and Te are not strictly coupled in their chemical behaviour, they are generally seen as related chalcophile semi-metals in mantle petrology (e.g., Lorand & Alard, 2010; Brenan, 2015). The partition coefficient for D_{Te}/D_{Se} between Mss and silicate is ~ 0.5-0.8 (Brenan, 2015). During sulphide liquid cooling and fractionation, Te preferentially enters the Iss portion. This could have the effect of increasing Se/Te ratio during early sulphide fractionation, however we can discount this as there is no correlation (or if anything a weak anti-correlation) between Te and Cu for both BMS groups (Fig. 11d).

By recalculating the bulk rock PGE and Au abundances of xenolith LR80 (from the analyses of a 5 g aliquot of powder from the unaltered core of the xenolith; Hughes *et al.*, 2014) to 100% sulphide (assuming a mean sulphide abundance of 0.07% for LR80, Table 4; using the method outlined by Huminicki *et al.*, 2005) and comparing this to the mean PGE and Au normalised patterns for Group A and B BMS, we observe that the bulk rock PGE abundances are controlled by BMS (Fig. 12). However, the bulk rock abundance of Au exceeds that present in the BMS and cannot be explained by this approach (Fig. 12).

Recent interpretations of chromatographic metasomatism in mantle xenoliths from the Svalbard Archipelago may provide an analogue for Au-depletion elsewhere in the northern European lithospheric mantle (Saunders *et al.*, 2015). In the Svalbard 'Group II' and 'Group III' xenoliths, BMS (particularly 'Group III-type 2 sulphides') have systematically low Au concentrations. It is suggested that these samples were situated closest to a conduit in the SCLM, through which carbonate-associated melt passed, resulting in the partitioning of Au into the fluid phase of this metasomatic agent and thus depletion of Au in BMS in the immediate vicinity of the conduit (Saunders *et al.*, 2015). Given the clear carbonate-phosphate-sulphide association in Group B BMS at Loch Roag, the low Au content in these samples may similarly be a result of extensive equilibration with such a metasomatic fluid, but this does not explain the differing PGE abundances of the *co-existing* Loch

Roag BMS of Group A and B. In particular the Group B BMS are extremely PGE-rich (particularly IPGE-rich) which is strikingly different from the low PGE abundance of the conduit-proximal metasomatic BMS in Svalbard Group III xenoliths (Saunders *et al.*, 2015). Similarly, it may not explain the depletion in Au also observed in Loch Roag Group A BMS grains (e.g., Fig. 12). We do not observe a depletion in the whole-rock abundance of Au, yet a depletion in Au is apparent by *in situ* analyses of the sulphides, consistently coupled with low Te contents for both groups of Loch Roag BMS (typically 1-10 ppm Te in LR80 BMS in comparison to up to 60 ppm in Svalbard Group III sulphides, Saunders *et al.*, 2015). Therefore we suggest that Au has not been stripped from the Loch Roag SCLM. This 'invisible' Au could instead be hosted by a sulphide population unrecorded by SEM or LA-ICP-MS, or more likely a non-sulphide mineral phase, probably interstitial to silicates – an idea supported by the discovery of nano-inclusions of Au in strained olivine crystal margins in Pyrenean lherzolites (Ferraris & Lorand, 2014). Au readily forms telluride minerals and the low Te content of the BMS may be linked to this 'invisible' Au fraction (i.e., as micro-phases of Au-tellurides).

4.2 A multi-metasomatic record of the lithospheric mantle at the margin of the North Atlantic Craton

The Scottish margin of the NAC became separated from Greenland during Palaeogene rifting (e.g., Saunders *et al.*, 1997). The Loch Roag dyke was intruded at 45.2 Ma (Faithfull *et al.*, 2012). Prior to this, Scotland was affected by Permo-Carboniferous rifting that formed alkali basaltic and lamprophyric magmas (Upton *et al.,* 2004), some of which host mantle xenolith suites such as at Rinibar (see Fig. 1 and Hughes *et al.*, 2016). Caledonian subduction beneath the southwestern margin of the NAC in Scotland culminated in a sequence of arc-related magmatic and hydrothermal episodes (see Strachan *et al.,* 2002 and references therein) and the formation of mixed 'appinitic' (biotite-hornblende diorites) and high Ba-Sr granitoid intrusions (e.g., Fowler *et al.*, 2008). Older magmatic events in northern Scotland include those associated with the West Highland Granite

Gneiss c. 870 Ma and which probably formed as a result of crustal extension (Fowler *et al.,* 2013); Palaeoproterozoic orogenesis, arc accretion and magmatism of the Laxfordian event c. 1.67-1.90 Ga (cf. Goodenough *et al.,* 2013 and references therein, and van Gool *et al.,* 2002) and Palaeoproterozoic extension and rifting forming the c. 2.4 Ga Scourie Dyke Swarm. Therefore, the lithospheric keel underlying Loch Roag and the wider Lewisian (NAC) of Scotland has experienced a series of tectono-magmatic and metasomatic events, some or all of which may have modified its 'sulphur-budget' (Hughes *et al.*, 2016). The two BMS populations in the Loch Roag peridotite xenoliths likely record some of these events.

Hughes *et al.* (2015b, 2016) compared the metasomatic clinopyroxene compositions, bulk rock geochemistry, and sulphide populations across numerous Scottish mantle xenoliths. The Loch Roag and Rinibar spinel lherzolite suites represent snap-shots of the lithospheric mantle composition from two different tectono-magmatic events (Eocene and Permo-Carboniferous, respectively) but the occurrence of Pt-sulphides in BMS associated with carbonates and phosphate occurs in both. Combined with similarities in metasomatic clinopyroxene compositions, Hughes *et al.* (2015b, 2016) suggested that this carbonate-phosphate-sulphide metasomatism recorded in both the Rinibar and Loch Roag xenoliths must pre-date the Eocene, and probably also pre-date the Permo-Carboniferous rifting that formed the Rinibar dyke.

If this argument is correct then it conceivably leaves the following older magmatic events as responsible for formation of carbonate-associated BMS (Group B in Loch Roag) under northern Scotland: (i) the Palaeoproterozoic extension event associated with the (c. 2.4 Ga) Scourie Dykes; (ii) Laxfordian orogenesis (1.67-1.90 Ga); (iii) Neoproterozoic rifting associated with the break-up of Rodinia (e.g., c. 870 Ma for the West Highland Granite Gneiss); and (iv) Caledonian orogenesis (subduction of the Iapetus Oceanic crust in the Grampian event c. 470 Ma with Scandian continent-continent collision c. 430 Ma). The only known carbonatite in the UK occurs at Loch Urigill (near Assynt, NW Scotland) and is dated at 429.2 ± 0.5 Ma (Goodenough *et al.*, 2011). Clinopyroxene Sr-,

Nd, and Hf-isotopes from Rinibar and Streap Com'laidh spinel lherzolite xenoliths have been used to infer carbonatitic metasomatism in the lithospheric mantle c. 550 ± 50 Ma, thought to relate to the opening of the Iapetus Ocean following the break-up of Rodinia (Bonadiman *et al.*, 2008). Further, time-integrated Sr- and Nd-isotopes from Long *et al.* (1991) for Loch Roag spinel lherzolite and pyroxenites xenoliths highlighted a carbonatitic metasomatic event c. 2.5-2.0 Ga. Hughes *et al.* (2014) suggested that the timing of this earlier carbonatite event could be related to the Scourie Dyke Swarm (c. 2.4 Ga). Carbonatite intrusions are well documented in the western Greenlandic portions of the NAC by Larsen & Rex (1992) who recognised five carbonatite-kimberlite-lamprophyre events: (a) c. 2.6 Ga, (b) c. 1.7-1.9 Ga (Ketilidian and Nagssugtoqidian mobile belts), (c) c. 1.1-1.3 Ga (associated with the Gardar magmatic province), (d) c. 600 Ma and (e) c. 169-176 Ma (Qaqarssuk carbonatite complex). Whilst the 1.7-1.9 Ga group of intrusions in west Greenland do not include carbonatites, carbonatites make up a significant portion of magmatic rocks in the other four events. Given the common occurrence of Pt-sulphides and carbonate-phosphate immiscibility in the Rinibar xenoliths, it is very unlikely that the Pt-rich sulphide-carbonate-phosphate Group B BMS of Loch Roag would be related to the Mesozoic Qaqarssuk carbonatitic event in west Greenland. Instead this three-way immiscibility event recorded in the Scottish lithospheric mantle could be related to either the c. 2.6 Ga or c. 600 Ma events recorded in Greenland, or more likely the Caledonian Loch Urigill carbonatite on the northern Highland mainland adjacent to the Hebridean Terrane in which the Loch Roag xenolith suite occurs. Nonetheless, the apparent unequilibrated textures (exsolutions and irregular grain boundaries) of the spinel-feldspar symplectites, in which Group B BMS are hosted, may be expected to have recrystallised to textures with low surfaced-to-volume ratios at mantle temperature conditions, and therefore could reflect a more recent metasomatic event in the Loch Roag xenoliths. Thus, together with Rinibar, this could indicate multiple sulphide-carbonate-phosphate events recorded in the northern Scottish SCLM.

Irrespective of the exact timing of the Pt-enriched sulphide-carbonate-phosphate immiscibility event that formed Group B BMS in Loch Roag spinel lherzolites, the occurrence of a PGE-rich population of

BMS in spinel-feldspar symplectites has important implications for understanding the regional controls on precious metal mineralisation. Hughes *et al.* (2015a) documented a temporal change in Pt/Pd ratio of North Atlantic Igneous Province basaltic lavas, such that the earliest lavas were Pt-rich (with a broadly chondritic Pt/Pd ratio ~ 1.8) while the youngest lavas on Iceland were comparatively Pd-rich (Pt/Pd ratio ~ 0.4). Hughes *et al.* (2015a) considered it likely that this early Pt-enrichment could reflect 'contamination' of ascending plume-derived magmas by lithospheric mantle BMS. This is particularly the case for PGE-rich and Pt-sulphide-bearing Group B BMS situated within spinel-feldspar symplectites that could be easily remobilised and assimilated by hot, ascending magmas. Thus the tectono-magmatic history, as recorded by BMS for chalcophile elements in the lithospheric mantle, may be a useful tool towards understanding the inherent geochemical 'fingerprints' of large igneous provinces and magmatic-hydrothermal mineralising systems on a regional scale (e.g., De Wit & Thiart, 2003; Groves *et al.*, 2005; Maier & Groves, 2013; Hughes *et al.*, 2016).

5. Conclusions

1. Detailed petrography reveals two populations of metasomatic BMS co-existing within a single mantle spinel lherzolite xenolith (LR80) from Loch Roag, NW Scotland. Using a combined approach to discriminate between these populations according to BMS texture, petrographic setting and *in situ* BMS trace element composition, we can recognise these BMS groups in other Loch Roag xenoliths.
2. Given their distinct petrographic setting (i.e., interstitial to silicate grain boundaries vs. within spinel-feldspar symplectite pockets), we can infer a relative chronology of BMS groups with differing PGE and $(Re/Os)_N$ systematics:
    a. The oldest BMS (Group A) have lowest total PGE abundances and highest $(Re/Os)_N$ ratios;
    b. The youngest BMS (Group B) contain micron-scale Pt-sulphide (cooperite), have the highest total PGE abundance (particularly enriched in IPGE), lowest $(Re/Os)_N$, and are associated with a three-way immiscibility between carbonate-sulphide-phosphate fluids/melts.
3. Tellurium is systematically depleted in all Loch Roag BMS and, combined with discrepancies between the measured *in situ* abundance of Au in BMS and the bulk rock Au concentration, we suggest that Au-tellurides may be present as discrete interstitial phases in these mantle xenoliths.
4. Based on similarities to other mantle xenolith suites in northern Scotland (hosted in older Permo-Carboniferous dykes), we suggest that the carbonatite-related event that formed Group B BMS is pre-Carboniferous.
5. Using an integrated *in situ* petrographic and bulk geochemical approach to establish the distinct precious metal budgets of BMS populations present within the lithospheric mantle (via mantle xenoliths) we provide a temporal insight into the metallogeny of the mantle and

its contribution to the metallogenesis of mantle-derived liquids during tectono-magmatic events.

Acknowledgements

Much of the Loch Roag material (xenolith and dyke) used throughout this study is from B.G.J. Upton's personal collection, now held at the British Geological Survey (BGS), Murchison House, Edinburgh. The BGS, particularly Michael Togher, is thanked for the curation, access and use of these samples. Anthony Oldroyd is thanked for his preparation of polished thin sections and Peter Fisher and Duncan Muir for their assistance and guidance at Cardiff University's SEM facilities. H.S.R. Hughes was funded by the Natural Environment Research Council (NERC) studentship NE/J50029X at the time of data collection, and is currently funded by the Claude Leon Foundation and supported by the DST-NRF CIMERA Centre of Excellence at the University of the Witwatersrand. NERC are thanked for funding open access publication of this paper. Parts of this work were funded by NERC SoS Consortium grant NE/M011615/1 "Te and Se Cycling and Supply" awarded to Cardiff University. Judith Coggon and Ambre Luguet are gratefully thanked for their constructive feedback on an earlier version of this manuscript. The authors are indebted to Sonja Aulbach and Jacek Puziewicz for their detailed and helpful reviews. Any remaining errors or misinterpretations are solely the responsibility of the authors.

Figure Captions

Figure 1 – (a) Map of Scottish lithospheric terranes, as delineated by major crustal lineaments. Major mantle xenolith localities marked, and labelled for Loch Roag (LR), Rinibar (RNB) and Streap Com'laidh (STP). Adapted from Upton *et al.* (2011). (b) Map of Scotland in the wider North Atlantic showing cratonic correlations of the North Atlantic Craton and bounding orogenic belts (Nagssugtoqidian and Ketillidian) to the north and south. Note that due to extensive Palaeoproterozoic reworking, the Lewisian of Scotland (north of the Great Glen Fault) is delineated as 'Nagssugtoqidian'.

Figure 2 – (a) Hand specimen (rock slice) photograph of LR80 showing orange-green alteration halo around the outer edge of the xenolith, and grey 'unaltered' core. Positions of a selection of thin sections (and corresponding polished blocks) marked. (b) and (c) show scanning electron microscrope (SEM) back-scattered electron (BSE) images of some spinel-feldspar symplectites in thin xenolith. Spinel is skeletal and surrounded by feldspar. The wide line in (c) is a laser ablation line. White arrows point to 'atoll-like' chromite within the symplectite.

Figure 3 – Bulk rock geochemistry (from Hughes *et al.*, 2015). Green squares are bulk analyses of various spinel lherzolite xenoliths from the Loch Roag suite. LR80 is labelled as this was the only xenolith large enough to allow for the grey 'unaltered' core of the xenolith to be crushed and analysed (smaller xenoliths incorporated some portion of green alteration halo). Crossed symbols show data from the western edge of the North Atlantic Craton in Greenland (Wittig *et al.*, 2010). White-filled circle denoted primitive upper mantle (PUM) from McDonough & Sun (1995). (a) Cr/Al ratio vs. Al/Si ratio. (b) Ca/Si ratio vs. Al/Si ratio. (c) Cu (anhydrous) vs. Cr/Al ratio.

Figure 4 – Reflected light photomicrographs of Loch Roag spinel lherzolite xenolith base metal sulphides (BMS). (a) and (b) show Group A BMS, interstitial to olivine, clinopyroxene and orthopyroxene. (c) Skeletal spinel in feldspar symplectite with inclusion-bearing Group B BMS and

other inclusion-free bearing BMS. (d) Spinel-feldspar symplectite with finer BMS within and directly adjacent to the symplectite. Note the elongate recrystallised crystals of clinopryoxene and very fine BMS associated with this (right of image).

Figure 5 – SEM BSE images of Group A BMS. (a) Close-up of metasomatic textures of intergrown pentlandite-pyrrhotite (Pn-Po) or Mss, chalcopyrite-pentlandite (Cp-Pn), and chalcopyrite with 'cross-hatched' textures. (b) Similar example of metasomatic BMS textures, as in (a). (c) Pentlandite (Pn) and Mss-rich (Pn-Po) example.

Figure 6 - SEM BSE images of Group B BMS. (a) Spinel-feldspar symplectite with Group B BMS within it. Note that line is a laser ablation line. (b) Close-up of BMS in (a) showing rounded globular texture of sulphides. (c) Rounded Group B BMS with PtS (cooperite) as discrete micron-sized phase within the chalcopyrite and at the margin of the BMS. Also minor galena (Ga) noted. (d) Close-up of PtS in (c). (e) and (f) Inclusion-rich Group B BMS. Rounded inclusions are calcite ($CaCO_3$) whereas more angular inclusions are serpentine (Serp).

Figure 7 - SEM BSE images of Group B BMS associated with a discontinuous vein of apatite through LR80. (a) Spongy $CaCO_3$ inclusion-rich apatite (Apt) surrounded by feldspar in vein through olivine (Ol). Note rounded BMS associated with vein and patches of $CaCO_3$ outwith the apatite and associated with feldspar. (b) Close-up of BMS in (a) showing rounded globular shape and inclusion of apatite within BMS. (c) Close-up of spongy apatite in vein. Abundant rounded inclusions of $CaCO_3$ and (now) voids. Micron-scale Ni-Fe sulphide droplets labelled within spongy apatite.

Figure 8 - µCT scan 3D reconstructions of portions of xenolith LR80. (a) Example of a 2D data slice (1 voxel in thickness) of the µCT scan of a 5mm core of LR80. A stack of these for the entire volume of the xenolith was built in order to facilitate 3D reconstruction and visualisation. (b) to (c) shows a sequence of frozen 3D frames of part of a slice of LR80 (approximately 2.5 cm long). The outer surface of the rock scanned is shown in (b) as a semi-transparent white shell. This is gradually

removed by increasing transparency of the xenolith (white shell) revealing the spinel (as the higher density mineral phase, along with a minor iron oxide veinlet) highlighted in blue in (c). (d) Freeze-frame of 3D-recontructed µCT data density filtered to show spinel (in blue). Note that the small density contrast between spinel and iron oxide (which occurs as a minor discontinuous veinlet in one peripheral area of the scanned xenolith) means that this image includes a minor zone of iron oxide (labelled on figure). (e) Same 3D dataset as (d) with showing lowest density phases (feldspar) in transparent colour shells. Interconnected feldspar is shown in the same colour (i.e., the green-blue shading delineates one set of interconnected feldspar, as does the brown, grey-green, pale blue and red. Field of view (at front of frame) in (d) and (e) is approximately 5mm wide.

Figure 9 – *In situ* major element data for BMS (from LA-ICP-MS). (a) Metal/S ratio vs. Fe/(Fe+Ni+Cu). (b) Metal/S ratio vs. Ni/(Ni+Cu+Fe). (c) Metal/S ratio vs. Cu/Cu+Ni+Fe). (d) Total PGE vs. Cu. Data are separated according to Group A and Group B BMS.

Figure 10 - *In situ* LA-ICP-MS data for Group A and Group B BMS end-member sulphide minerals (a), all Group A BMS data (b) and all Group B BMS data (c).

Figure 11 – *In situ* major and trace element data for BMS (from LA-ICP-MS). (a) $(Pd/Ir)_N$ vs $(Os/Ir)_N$. (b) Cu vs. $(Re/Os)_N$. (c) S/Se vs. Te. (d) Te vs Cu.

Figure 12 – Mass balance for bulk rock PGE and Au abundances measured in LR80 (from Hughes *et al.*, 2014) recalculated to 100% sulphide (using the method outlined by Huminicki *et al.*, 2005) and normalised to chondrite for comparison to the mean PGE and Au of normalised values of Group A and Group B BMS (from LA-ICP-MS). Os is removed from this plot because of its potential volatilisation during fire assay (for bulk rock analyses).

Table Captions

Table 1 – Bulk rock major and trace element compositions of spinel lherzolite xenolith ('unaltered' grey core) LR80 and the monchiquite dyke host to the Loch Roag xenolith suite. See Hughes *et al.* (2014) for details.

Table 2 – Mean BMS major element compositions for Group A and B (with and without carbonate inclusions) compiled from quantitative SEM data in Supplementary Material (as a series of spot analyses for each sulphide component (chalcopyrite, pentlandite and pyrrhotite, or pyrrhotite and pentlandite in fine Mss intergrowths) per BMS group – i.e., Group A, B).

Table 3 – Mean BMS compositions for Group A and B (with and without carbonate inclusions) compiled from full LA-ICP-MS dataset in Supplementary Material (including all major elements as measured by LA-ICP-MS). **S indicates that S was used for calibration of LA-ICP-MS results by quantitative EDS SEM spot analyses of corresponding points. * for Ru, Rh and Pd indicates abundances are reported for the element and have been corrected for isotope overlaps with argide species.

Table 4 – Modal abundance (by area %) of minerals in 3 thin section of LR80. See main text (methods) for details of calculation.

Table 5 – Group A and Group B (both carbonate and non-carbonate inclusion-bearing) BMS characteristics in terms of size, mineral associations and end-member sulphide abundances.

References

Agrosì, G., Nestola, F., Tempesta, G., Bruno, M., Scandale, E. and Harris, J., 2016. X-ray tomographic study of a diamond from Udachnaya: Implications for the genetic nature of inclusions. Lithos, 248, pp.153-159.

Alard, O., Griffin, W. L., Lorand, J. -P., Jackson, S. E. & O'Reilly, S. Y. 2000. Non-chondritic distribution of the highly siderophile elements in mantle sulphides. Nature, 407, 891-894.

Alard, O., Griffin, W. L., Pearson, N. J., Lorand, J. -P. & O'Reilly, S. Y. 2002. New insights into the Re-Os systematics of sub-continental lithospheric mantle from in situ analysis of sulphides. Earth and Planetary Science Letters, 203, 651-663.

Alard, O., Luguet, A., Pearson, N. J., Griffin, W. L., Lorand, J. -P., Gannoun, A., Burton, K. W. & O'Reilly, S. Y. 2005. In situ Os isotopes in abyssal peridotites bridge the isotopic gap between MORBs and their source mantle. Nature, 436, 1005-1008.

Alard, O., Lorand, J. -P., Reisberg, L., Bodinier, J. -L., Dautria, J. -M. & O'Reilly, S. Y. 2011. Volatile-rich metasomatism in Montferrier xenoliths (Southern France): Implications for the abundances of chalcophile and highly siderophile elements in the subcontinental mantle. Journal of Petrology, 52, 2009-2045.

Arndt, N. T. 2013. The lithospheric mantle plays no active role in the formation of orthomagmatic ore deposits. Economic Geology, 108, 1953-1970.

Aulbach, S., Griffin, W. L., Pearson, N. J., O'Reilly, S. Y., Kivi, K. & Doyle, B. J. 2004. Mantle formation and evolution, Slave Craton: constraints from HSE abundances and Re–Os isotope systematics of sulfide inclusions in mantle xenocrysts. Chemical Geology, 208, 61-88.

Aulbach, S., Creaser, R.A., Pearson, N.J., Simonetti, S.S., Heaman, L.M., Griffin, W.L. and Stachel, T., 2009. Sulfide and whole rock Re–Os systematics of eclogite and pyroxenite xenoliths from the Slave Craton, Canada. Earth and Planetary Science Letters, 283(1), 48-58.

Aulbach, S., Mungall, J.E. and Pearson, D.G. 2016. Distribution and processing of highly siderophile elements in cratonic mantle lithosphere. Reviews in Mineralogy and Geochemistry, 81(1), 239-304.

Baba, S., 2002. Tectono-metamorphic events in the North Atlantic region in the Palaeoproterozoic from the view point of high-grade metamorphic rocks in the Lewisian Complex, South Harris, NW Scotland. Gondwana Research,5(4), 757-770.

Bedini, R.M., Bodinier, J.L., Dautria, J.M. and Morten, L., 1997. Evolution of LILE-enriched small melt fractions in the lithospheric mantle: a case study from the East African Rift. Earth and Planetary Science Letters, 153(1), 67-83.

Bonadiman, C., Coltorti, M., Duggen, S., Paludetti, L., Siena, F., Thirlwall, M. F. & Upton, B. G. J. 2008. Palaeozoic subduction-related and kimberlite or carbonatite metasomatism in the Scottish lithospheric mantle. In: Metasomatism in Oceanic and Continental Lithospheric Mantle. (eds. Coltorti, M. & Gregoire, M.), 303-333. Special Publication 293. Geological Society of London.

Brenan, J.M., 2015. Se–Te fractionation by sulfide–silicate melt partitioning: implications for the composition of mantle-derived magmas and their melting residues. Earth and Planetary Science Letters, 422, 45-57.

Bridgwater, D., Watson, J. & Windley, B. F. 1973. The Archaean Craton of the North Atlantic Region. Philosophical Transactions of the Royal Society A: Mathematical, Physical and Engineering Sciences, 273, 493-512.

Burton, K.W., Schiano, P., Birck, J.L. and Allegre, C.J., 1998. The behaviour of Re and Os in mantle minerals with the implications for mantle melting. EOS transaction. American Geophysical Union, 79(46), S373.

Carlson, W.D., Denison, C. and Ketcham, R.A., 2000. High-resolution X-ray computed tomography as a tool for visualization and quantitative analysis of igneous textures in three dimensions. Visual Geosciences, 4(3), 1-14.

Davies, J. H. F. L. & Heaman, L. M. 2014. New U-Pb baddeleyite and zircon ages for the Scourie dyke swarm: A long-lived large igneous province with implications for the Paleoproterozoic evolution of NW Scotland. Precambrian Research, 249, 180-198.

Delpech, G., Lorand, J. -P., Gregoire, M., Cottin, J. -Y., O'Reilly, S. Y. 2012. In-situ geochemistry of sulfides in highly metasomatized mantle xenoliths from Kerguelen, southern Indian Ocean. Lithos, 154, 296-314.

Denison, C. and Carlson, W.D., 1997. Three-dimensional quantitative textural analysis of metamorphic rocks using high-resolution computed X-ray tomography: Part II. Application to natural samples. Journal of Metamorphic Geology, 15(1), 45-57.

Downes, H., de Vries, C. and Wittig, N., 2015. Hf–Zr anomalies in clinopyroxene from mantle xenoliths from France and Poland: implications for Lu–Hf dating of spinel peridotite lithospheric mantle. International Journal of Earth Sciences, 104(1), 89-102.

Dromgoole, E. L., & Pasteris, J. D. 1987. Interpretation of the sulfide assemblages in a suite of xenoliths from Kilbourne Hole, New Mexico. Geological Society of America Special Papers, 215, 25-46.

Eggler, D.H. and Lorand, J.P., 1993. Mantle sulfide geobarometry. Geochimica et Cosmochimica Acta, 57(10), 2213-2222.

Faithfull, J. W., Timmerman, M. J., Upton, B. G. J. & Rumsey, M. S. 2012. Mid-Eocene renewal of magmatism in NW Scotland: the Loch Roag Dyke, Outer Hebrides. Journal of the Geological Society, 169, 115-118.

Ferraris, C. & Lorand, J. -P. 2014. Novodneprite ($AuPb_3$), anyuiite [$Au(Pb, Sb)_2$] and gold micro- and nano-inclusions within plastically deformed mantle-derived olivine from the Lherz peridotite (Pyrenees, France): a HRTEM–AEM–EELS study. Physics and Chemistry of Minerals, 42(2), 143-150.

Fonseca, R.O., Laurenz, V., Mallmann, G., Luguet, A., Hoehne, N. and Jochum, K.P., 2012. New constraints on the genesis and long-term stability of Os-rich alloys in the Earth's mantle. Geochimica et Cosmochimica Acta, 87, 227-242.

Fowler, M. B., Kocks, H., Darbyshire, D. P. F. & Greenwood, P. B. 2008. Petrogenesis of high Ba-Sr plutons from the Northern Highlands Terrane of the British Caledonian Province. Lithos, 105, 129-148.

Fowler, M., Millar, I. L., Strachan, R. A. & Fallick, A. E. 2013. Petrogenesis of the Neoproterozoic West Highland Granitic Gneiss, Scottish Caledonides: Cryptic mantle input to S-type granites? Lithos, 168-169, 173-185.

Gillespie, M. and Styles, M., 1999. BGS rock classification scheme, Volume 1. Classification of igneous rocks.

Godel, B., 2013. High-resolution X-ray computed tomography and its application to ore deposits: From data acquisition to quantitative three-dimensional measurements with case studies from Ni-Cu-PGE deposits. Economic Geology, 108(8), 2005-2019.

Godel, B., Barnes, S.J. and Maier, W.D., 2006. 3-D distribution of sulphide minerals in the Merensky Reef (Bushveld Complex, South Africa) and the JM Reef (Stillwater Complex, USA) and their relationship to microstructures using X-ray computed tomography. Journal of Petrology, 47(9), 1853-1872.

González-Jiménez, J.M., Griffin, W.L., Gervilla, F., Proenza, J.A., O'Reilly, S.Y. and Pearson, N.J., 2014. Chromitites in ophiolites: How, where, when, why? Part I. A review and new ideas on the origin and significance of platinum-group minerals. Lithos, 189, 127-139.

González-Jiménez, J.M., Villaseca, C., Griffin, W.L., O'Reilly, S.Y., Belousova, E., Ancochea, E. and Pearson, N.J., 2014. Significance of ancient sulphide PGE and Re-Os signatures in the mantle beneath Calatrava, Central Spain. Contributions to Mineralogy and Petrology, 168, 1-24.

Goodenough, K. M., Millar, I., Strachan, R. A., Krabbendam, M. & Evans, J. A. 2011. Timing of regional deformation and development of the Moine Thrust Zone in the Scottish Caledonides: constraints from the U-Pb geochronology of alkaline intrusions. Journal of the Geological Society, London, 168, 99-114.

Goodenough, K. M., Crowley, Q. G., Krabbendam, M. & Parry, S. F. 2013. New U-Pb age constraints for the Laxford Shear Zone, NW Scotland: Evidence for tectono-magmatic processes associated with the formation of a Paleoproterozoic supercontinent. Precambrian Research, 233, 1-19.

Grégoire, M., Moine, B.N., O'Reilly, S.Y., Cottin, J.Y. and Giret, A., 2000. Trace element residence and partitioning in mantle xenoliths metasomatized by highly alkaline, silicate-and carbonate-rich melts (Kerguelen Islands, Indian Ocean). Journal of Petrology, 41(4), 477-509.

Griffin, W.L., Spetsius, Z.V., Pearson, N.J. and O'Reilly, S.Y., 2002. In situ Re-Os analysis of sulfide inclusions in kimberlitic olivine: New constraints on depletion events in the Siberian lithospheric mantle. Geochemistry, Geophysics, Geosystems, 3(11), 1-25.

Griffin, W.L., Graham, S., O'Reilly, S.Y. and Pearson, N.J., 2004. Lithosphere evolution beneath the Kaapvaal Craton: Re–Os systematics of sulfides in mantle-derived peridotites. Chemical Geology, 208(1), 89-118.

Griffin, W.L., Begg, G. and O'Reilly, S.Y. 2013. Continental-root control on the genesis of magmatic ore deposits. Nature Geoscience, 6, 905-910.

Groves, D. I. & Bierlein, F. P. 2007. Geodynamic settings of mineral deposit systems. Journal of the Geological Society, London, 164, 19-30.

Groves, D. I., Ho, S. E., Rock, N. M. S., Barley, M. E. & Muggeridge, M. T. 1987. Archean cratons, diamond and platinum: Evidence for coupled long-lived crust-mantle systems. Geology, 15, 801-805.

Guo, J., Griffin, W. L. & O'Reilly, S. Y. 1999. Geochemistry and origin of sulphide minerals in mantle xenoliths: Qilin, Southeastern China. Journal of Petrology, 40, 1125-1149.

Harvey, J., Gannoun, A., Burton, K.W., Schiano, P., Rogers, N.W. and Alard, O., 2010. Unravelling the effects of melt depletion and secondary infiltration on mantle Re–Os isotopes beneath the French Massif Central. Geochimica et Cosmochimica Acta, 74(1), pp.293-320.

Helmy, H. M., Ballhaus, C., Berndt, J., Bockrath, C. & Wohlgemuth-Ueberwasser, C. 2007. Formation of Pt, Pd and Ni tellurides: experiments in sulfide-telluride systems. Contributions to Mineralogy and Petrology, 153, 577-591.

Holwell, D. A. & McDonald, I. 2010. A review of the behaviour of Platinum Group Elements within natural magmatic sulfide ore systems. Platinum Metals Review, 54, 26-36.

Holzheid, A., Sylvester, P., O'Neill, H. S. C., Rubie, D. C. & Palme, H. 2000. Evidence for a late chondritic veneer in the Earth's mantle from high-pressure partitioning of palladium and platinum. Nature, 406, 396-399.

Hughes, H. S. R., McDonald, I., Goodenough, K. M., Ciborowski, T. J. R., Kerr, A. C., Davies, J. H. F. L. & Selby, D. 2014. Enriched lithospheric mantle keel below the Scottish margin of the North Atlantic Craton: Evidence from the Palaeoproterozoic Scourie Dyke Swarm and mantle xenoliths. Precambrian Research, 250, 97-126.

Hughes, H. S. R., McDonald, I. & Kerr, A. C. 2015a. Platinum-group element signatures in the North Atlantic Igneous Province: Implications for mantle controls on metal budgets during continental breakup. Lithos. 233, 89-110.

Hughes, H. S. R., McDonald, I., Faithfull, J. W., Upton, B. G. J. & Downes, H. 2015b. Trace element abundances in the shallow lithospheric mantle of the North Atlantic Craton margin: Implications for melting and metasomatism beneath Northern Scotland. Mineralogical Magazine, 79(4), 877-907.

Hughes, H. S. R., McDonald, I., Faithfull, J. W. & Upton, B. G. J. 2016. Cobalt and precious metals in sulphides of peridotite xenoliths and inferences concerning their distribution according to geodynamic environment: A case study from the Scottish lithospheric mantle. Lithos. 240-243, 202-227.

Huminicki, M. A. E., Sylvester, P. J., Cabri, L. J., Lesher, C. M. & Tubrett, M. 2005. Quantitative mass balance of platinum group elements in the Kelly Lake Ni–Cu–PGE deposit, Copper Cliff offset, Sudbury. Economic Geology, 100, 1631-1646.

Hunter, R. H. & Upton, B. G. J. 1987. The British Isles - a Palaeozoic mantle sample. In: Mantle xenoliths. (ed. Nixon, P. H.), 107-118. Chichester: John Wiley.

Jacob, D.E., Wirth, R., Enzmann, F., Kronz, A. and Schreiber, A., 2011. Nano-inclusion suite and high resolution micro-computed-tomography of polycrystalline diamond (framesite) from Orapa, Botswana. Earth and Planetary Science Letters, 308(3), 307-316.

Jagoutz, E., Palme, H., Baddenhausen, H., Blum, K., Cendales, M., Dreibus, G., Spettel, B., Waenke, H. and Lorenz, V., 1979. The abundances of major, minor and trace elements in the Earth's mantle as derived from primitive ultramafic nodules. In Lunar and Planetary Science Conference Proceedings. 10, 2031-2050.

Ketcham, R.A. and Carlson, W.D., 2001. Acquisition, optimization and interpretation of X-ray computed tomographic imagery: applications to the geosciences. Computers & Geosciences, 27(4), 381-400.

Kinny, P. D., Friend, C. R. L. & Love, G. J. 2005. Proposal for a terrane-based nomenclature for the Lewisian Gneiss Complex of NW Scotland. Journal of the Geological Society, 162, 175-186.

Kondo, M., Tsuchiyama, A., Hirai, H. and Koishikawa, A., 1997. High resolution X-ray computed tomographic (CT) images of chondrites and a chondrule. Antarctic Meteorite Research, 10, 437.

Kyle, J.R. and Ketcham, R.A., 2003. In situ distribution of gold in ores using high-resolution X-ray computed tomography. Economic Geology, 98(8), 1697-1701.

Larsen, L. M. & Rex, D. C. 1992. A review of the 2500 Ma span of alkaline-ultramafic, potassic and carbonatitic magmatism in West Greenland. Lithos, 28, 367-402.

Long, A. M., Menzies, M. A., Thirlwall, M. F., Upton, B. G. J. & Apsen, P. 1991. Carbonatite-mantle interaction: A possible origin for megacryst/xenolith suites in Scotland. In: Meyer, H. O. A. & Leonardos, O. H. (eds.) Fifth International Kimberlite Conference. Brazil.

Lorand, J.-P., 1990. Are spinel lherzolite xenoliths representative of the abundance of sulfur in the upper mantle? Geochimica et Cosmochimica Acta, 54(5), pp.1487-1492.

Lorand, J. -P., & Conquere, F. 1983. Contribution à l'étude des sulfures dans les enclaves de lherzolite à spinelle des basaltes alcalins (Massif Central et Languedoc, France). Bulletin de Minéralogie, 106(5), 585-605.

Lorand, J. -P. & Alard, O. 2001. Platinum-group element abundances in the upper mantle: New constraints for in situ and whole-rock analyses of Massif Central xenoliths (France). Geochimica et Cosmochimica Acta, 65, 2789-2806.

Lorand, J.-P. & Gregoire, M., 2006. Petrogenesis of base metal sulphide assemblages of some peridotites from the Kaapvaal craton (South Africa). Contributions to Mineralogy and Petrology, 151(5), 521-538.

Lorand, J. -P. & Alard, O. 2010. Determination of selenium and tellurium concentrations in Pyrenean peridotites (Ariege, France): New insight into S/Se/Te systematics of the upper in mantle samples. Chemical Geology, 278, 120-130.

Lorand, J.-P. & Luguet, A., 2016. Chalcophile and siderophile elements in mantle rocks: Trace elements controlled by trace minerals. Reviews in Mineralogy and Geochemistry, 81(1), 441-488.

Lorand, J. -P., Alard, O., Luguet, A. & Keays, R. R. 2003. Sulfur and selenium systematics of the subcontinental lithospheric mantle: Inferences from the Massif Central xenolith suite (France). Geochimica et Cosmochimica Acta, 67, 4137-4151

Lorand, J. -P., Delpech, G., Gregoire, M., Moine, B., O'Reilly, S. Y. & Cottin, J. -Y. 2004. Platinum-group elements and the multistage metasomatic history of Kerguelen lithospheric mantle (South Indian Ocean). Chemical Geology, 208, 195-215.

Lorand, J. -P., Luguet, A., Alard, O., Bezos, A. & Meisel, T. 2008. Abundance and distribution of platinum-group elements in orogenic lherzolites; a case study in a Fontete Rouge lherzolite (French Pyrénées). Chemical Geology, 248, 174-194.

Lorand, J. -P., Luguet, A. & Alard, O. 2013. Platinum-group element systematics and petrogenetic processing of the continental upper mantle: A review. Lithos, 164-167, 2-21.

Luguet, A. & Reisberg, L., 2016. Highly Siderophile Element and ^{187}Os Signatures in Non-cratonic Basalt-hosted Peridotite Xenoliths: Unravelling the Origin and Evolution of the Post-Archean Lithospheric Mantle. Reviews in Mineralogy and Geochemistry, 81(1), 305-367.

Luguet, A., Lorand, J. -P. & Seyler, M. 2003. Sulfide petrology and highly siderophile element geochemistry of abyssal peridotites: a coupled study of samples from the Kane Fracture Zone (45°W 23°20N, MARK area, Atlantic Ocean). Geochimica et Cosmochimica Acta, 67, 1553-1570.

Luguet, A., Lorand, J.-P., Alard, O. & Cottin, J.Y., 2004. A multi-technique study of platinum group element systematic in some Ligurian ophiolitic peridotites, Italy. Chemical Geology, 208(1), 175-194.

Maier, W. D., Peltonen, P., McDonald, I., Barnes, S. J., Barnes, S. -J., Hatton, C. & Viljoen, F. 2012. The concentration of platinum-group elements and gold in southern African and Karelian kimberlite-hosted mantle xenoliths: Implications for the noble metal content of the Earth's mantle. Chemical Geology, 302-303, 119-135.

Marchesi, C., Garrido, C.J., Bosch, D., Bodinier, J.L., Gervilla, F. and Hidas, K., 2013. Mantle refertilization by melts of crustal-derived garnet pyroxenite: Evidence from the Ronda peridotite massif, southern Spain. Earth and Planetary Science Letters, 362, 66-75.

McDonough, W. F. & Sun, S. 1995. The Composition of the Earth. Chemical Geology, 120, 223-253.

Mees, F., Swennen, R., Van Geet, M. and Jacobs, P., 2003. Applications of X-ray computed tomography in the geosciences. Geological Society, London, Special Publications, 215(1), 1-6.

Menzies, M. & Halliday, A. 1988. Lithospheric mantle domains beneath the Archean and Proterozoic crust of Scotland. Journal of Petrology, Special Lithosphere Issue, 275-302.

Menzies, M.A. & Dupuy, C., 1991. Orogenic massifs: protolith, process and provenance. Journal of Petrology, (2), 1-16.

Menzies, M. A., Halliday, A. N., Palacz, Z., Hunter, R. N., Upton, B. G. J., Aspen, P. & Hawkesworth, C. J. 1987. Evidence from mantle xenoliths for an enriched lithospheric keel under the Outer Hebrides. Nature, 325, 44-47.

Mitchell, R. H. & Keays, R. R. 1981. Abundance and distribution of gold, palladium and iridium in some spinel and garnet lherzolites: implications for the nature and origin of precious metal-rich intergranular components in the upper mantle Geochimica et Cosmochimica Acta, 45, 2425-2442.

Moine, B., Gregoire, M., O'Reilly, S. Y., Delpech, G., Sheppard, S. M. F., Lorand, J. -P., Renac, C., Giret, A. & Cottin, J. -Y. 2004. Carbonatite melt in oceanic upper mantle beneath the Kerguelen Archipelago. Lithos, 75, 239-252.

Morgan, J.W., 1986. Ultramafic xenoliths: clues to Earth's late accretionary history. Journal of Geophysical Research: Solid Earth, 91(B12), 12375-12387.

Mungall, J. E., Andrews, D., Cabri, L., Sylvester, P. & Tubrett, M. 2005. Partitioning of Cu, Ni, Au, and platinum-group elements between monosulphide solid solution and sulphide melt under controlled oxygen and sulphur fugacities. Geochimica et Cosmochimica Acta, 69, 4349-4360.

Mungall, J. E. & Brenan, J. M. 2014. Partitioning of platinum-group elements and Au between sulfide liquid and basalt and the origins of mantle-crust fractionation of the chalcophile elements. Geochimica et Cosmochimica Acta, 125, 265-289.

Park, R. G. 1994. Early Proterozoic tectonic overview of the northern British Isles and neighbouring terrains in Laurentia and Baltica. Precambrian Research, 68, 65-79.

Park, R. G. 1995. Palaeoproterozoic Laurentia-Baltica relationships: a view from the Lewisian. In: Early Precambrian Processes. Geological Society Special Publication 95. (eds. Coward, M. P. & Ries, A. C.). The Geological Society, London, 95, 211-224.

Park, R. G. 2005. The Lewisian terrane model: a review. Scottish Journal of Geology, 41, 105-118.

Park, R. G. & Tarney, J. 1987. The Lewisian complex: a typical Precambrian high-grade terrain? In: Evolution of the Lewisian and Comparable Precambrian high grade terrains. (eds. Park, R. G. & Tarney, J.), 13-25. Special Publication of the Geological Society, 27, 13-25.

Pattou, L., Lorand, J. -P. & Gros, M. 1996. Non-chondritic platinum-group element ratios in the Earth's mantle. Nature, 379, 712-715.

Pearson, D. G., Canil, D. & Shirey, S. B. 2003. Mantle samples included in volcanic rocks: Xenoliths and diamonds. In: Treatise on Geochemistry. 171-275.

Peregoedova, A., Barnes, S.J. and Baker, D.R., 2004. The formation of Pt–Ir alloys and Cu–Pd-rich sulfide melts by partial desulfurization of Fe–Ni–Cu sulfides: results of experiments and implications for natural systems.Chemical Geology, 208(1), 47-264.

Powell, W. and O'Reilly, S., 2007. Metasomatism and sulfide mobility in lithospheric mantle beneath eastern Australia: implications for mantle Re–Os chronology. Lithos, 94(1), 132-147.

Prichard, H. M., Knight, R. D., Fisher, P. C., McDonald, I., Zhu, M. -F. & Wang, C. Y. 2013. Distribution of platinum-group elements in magmatic and altered ores in the Jinchuan intrusion, China: an example of selenium remobilization by postmagmatic fluids. Mineralium Deposita, 48, 767-786.

Rampone, E., Piccardo, G.B., Vannucci, R., Bottazzi, P. and Ottolini, L., 1993. Subsolidus reactions monitored by trace element partitioning: the spinel-to plagioclase-facies transition in mantle peridotites. Contributions to Mineralogy and Petrology, 115(1), 1-17.

Saunders, A. D., Fitton, J. G., Kerr, A. C., Norry, M. J. & Kent, R. W. 1997. The North Atlantic Igneous Province. In: Large Igneous Provinces: Continental, Oceanic, and Planetary Flood Volcanism. (eds. Mahoney, J. J. & Coffin, M. F.), 45-93. Washington DC: American Geophysical Union.

Saunders, J.E., Pearson, N.J., O'Reilly, S.Y. and Griffin, W.L., 2015. Sulfide metasomatism and the mobility of gold in the lithospheric mantle. Chemical Geology, 410, 149-161.

Schulze, D.J., Wiese, D. and Steude, J., 1996. Abundance and distribution of diamonds in eclogite revealed by volume visualization of CT X-ray scans. The Journal of Geology, 104, 109-114.

Smith, J. W., Holwell, D. A. & McDonald, I. 2014. Precious and base metal geochemistry and mineralogy of the Grasvally Norite-Pyroxenite-Anothosite (GNPA) member, northern Bushveld Complex, South Africa: implications for a multistage emplacement. Mineralium Deposita, 49, 667-692.

Strachan, R. A., Smith, M., Harris, A. L. & Fettes, D. J. 2002. The Northern Highland and Grampian terranes. In: Trewin, N. H. (ed.) The Geology of Scotland. The Geological Society.

Szabó, C. & Bodnar, R.J., 1995. Chemistry and origin of mantle sulfides in spinel peridotite xenoliths from alkaline basaltic lavas, Nógrád-Gömör Volcanic Field, northern Hungary and southern Slovakia. Geochimica et Cosmochimica Acta, 59(19), 3917-3927.

Upton, B. J. G., Aspen, P. & Chapman, N. A. 1983. The upper mantle and deep crust beneath the British Isles: evidence from inclusions in volcanic rocks. Journal of the Geological Society, 140, 105-121.

Upton, B. G. J., Hinton, R. W., Aspen, P., Finch, A. & Valley, J. W. 1999. Megacrysts and Associated Xenoliths: Evidence for Migration of Geochemically Enriched Melts in the Upper Mantle beneath Scotland. Journal of Petrology, 40, 935-956.

Upton, B. G. J., Stephenson, D., Smedley, P. M., Wallis, S. M. & Fitton, J. G. 2004. Carboniferous and Permian magmatism in Scotland. In: Permo-Carboniferous Magmatism and Rifting in Europe. (eds. Neumann, E.-R., Davies, G. R., Timmerman, M. J., Heeremans, M. & Larsen, B. T.). Special Publication of the Geological Society, 223, 195-218.

Upton, B. G. J., Downes, H., Kirstein, L. A., Bonadiman, C., Hill, P. G. & Ntaflos, T. 2011. The lithospheric mantle and lower crust-mantle relationships under Scotland: a xenolithic perspective. Journal of the Geological Society, 168, 873-886.

van Gool, J. A. M., Connelly, J. N., Marker, M. & Mengel, F. C. 2002. The Nagssugtoqidian Orogen of West Greenland: tectonic evolution and regional correlations from a West Greenland perspective. Canadian Journal of Earth Sciences, 39(5), 665-686.

Wainwright, A.N., Luguet, A., Fonseca, R.O.C. and Pearson, D.G., 2015. Investigating metasomatic effects on the ^{187}Os isotopic signature: A case study on micrometric base metal sulphides in metasomatised peridotite from the Letlhakane kimberlite (Botswana). Lithos, 232, 35-48.

Wittig, N., Webb, M., Pearson, D. G., Dale, C. W., Ottley, C. J., Hutchison, M., Jensen, S. M., Luguet, A. 2010. Formation of the North Atlantic Craton: Timing and mechanisms constrained from Re–Os isotope and PGE data of peridotite xenoliths from S.W. Greenland. Chemical Geology, 276, 166-187.

Zheng, J.P., Griffin, W.L., O'Reilly, S.Y., Yu, C.M., Zhang, H.F., Pearson, N. and Zhang, M., 2007. Mechanism and timing of lithospheric modification and replacement beneath the eastern North China Craton: peridotitic xenoliths from the 100 Ma Fuxin basalts and a regional synthesis. Geochimica et Cosmochimica Acta, 71(21), 5203-5225.

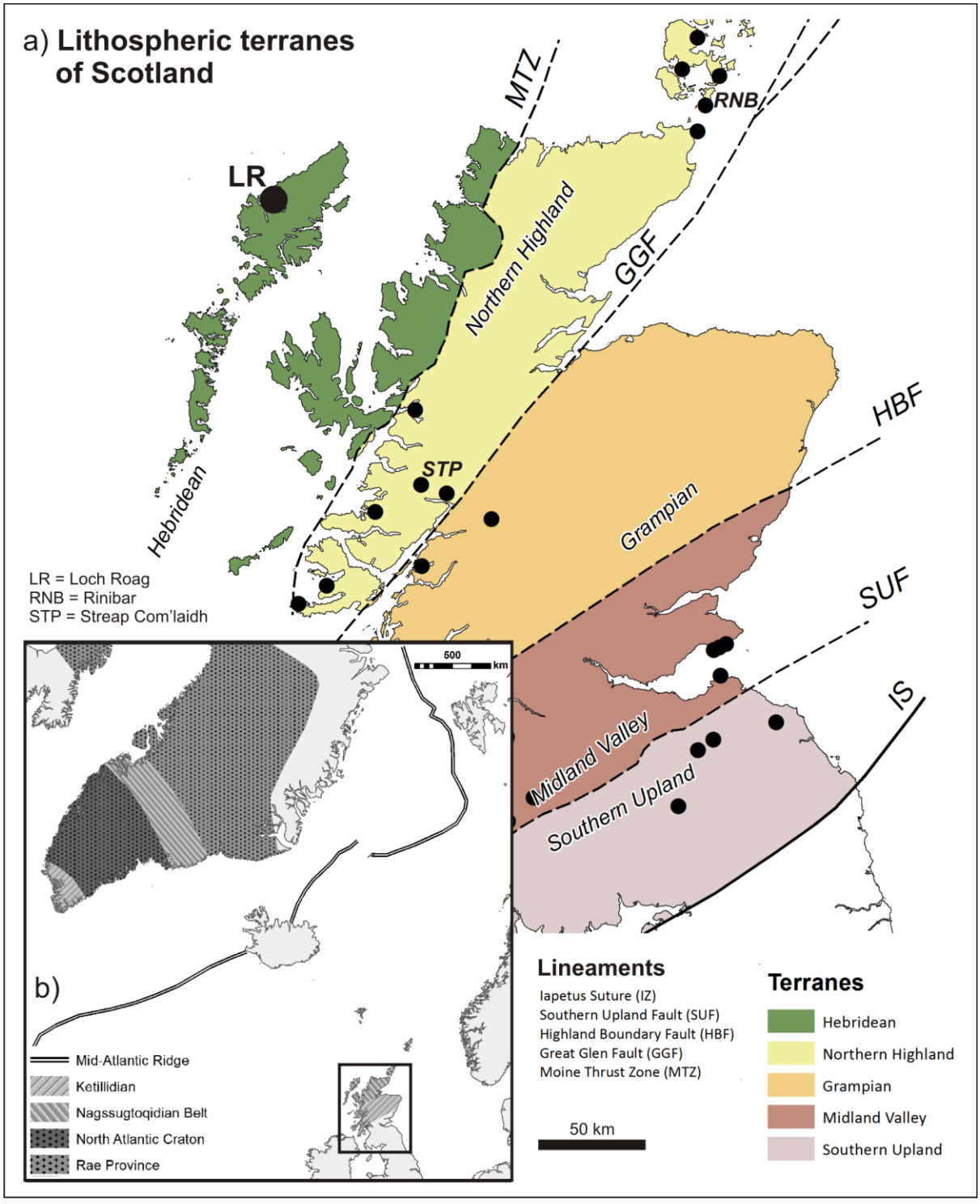

Figure 1

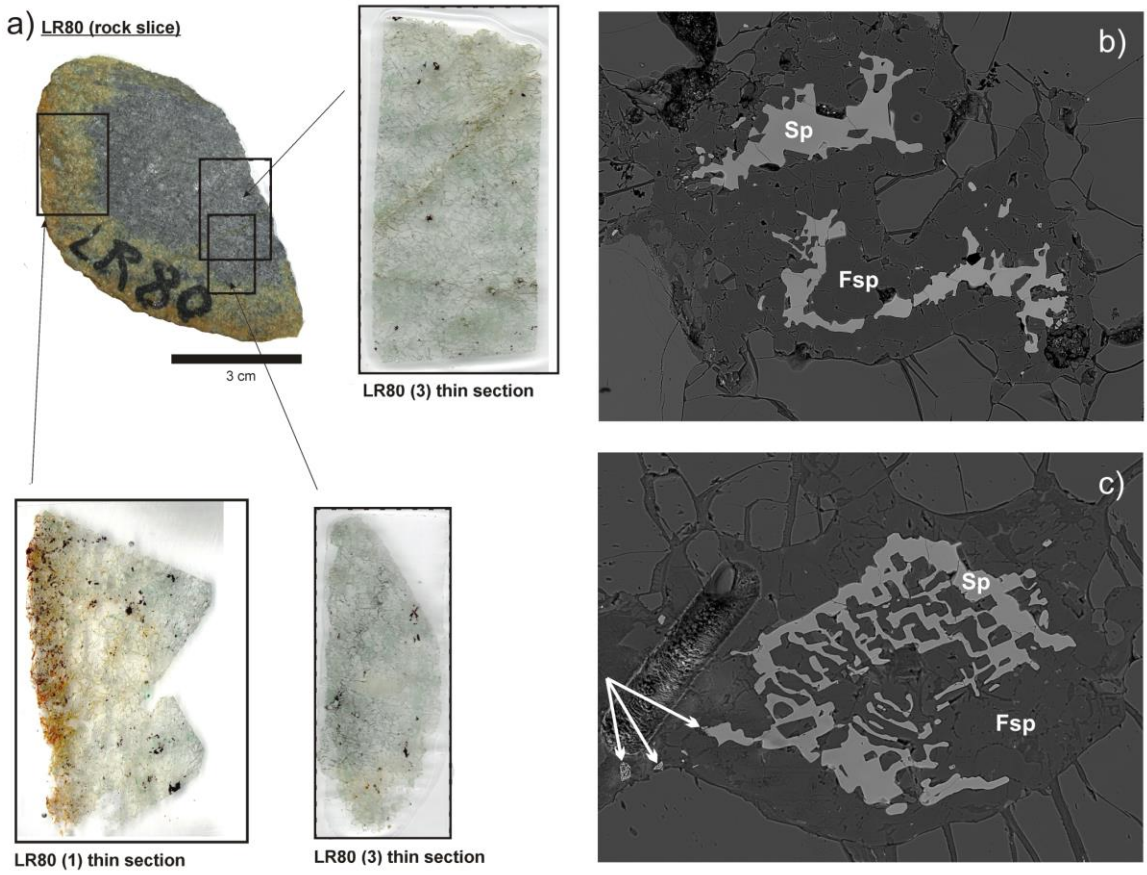

Figure 2

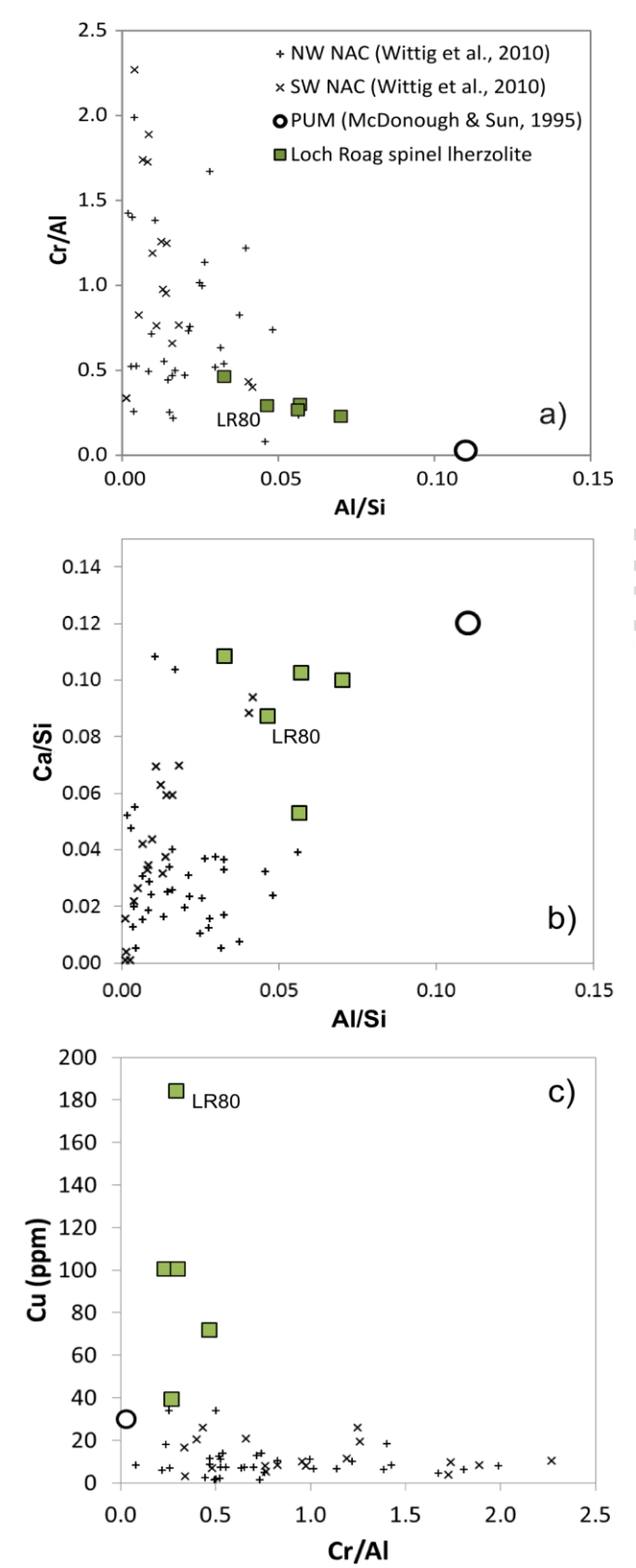

Figure 3

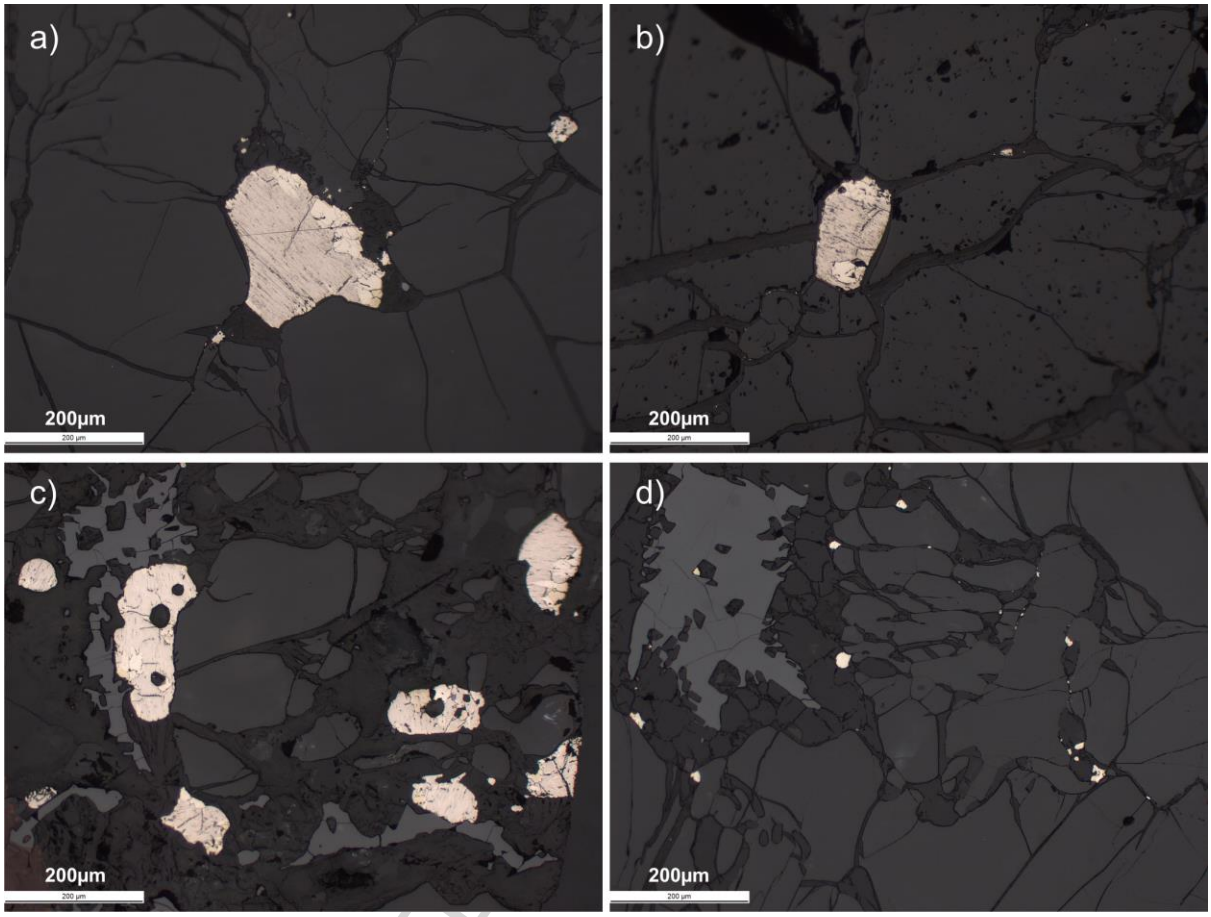

Figure 4

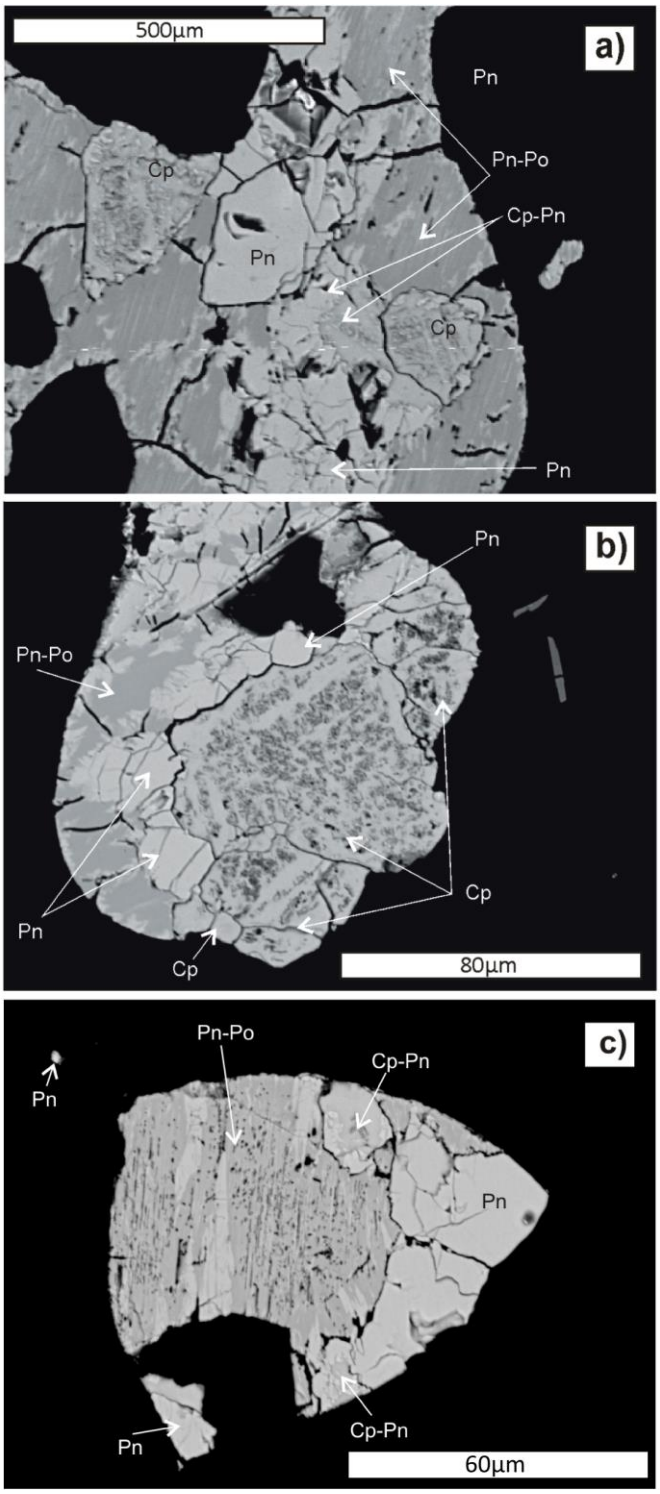

Figure 5

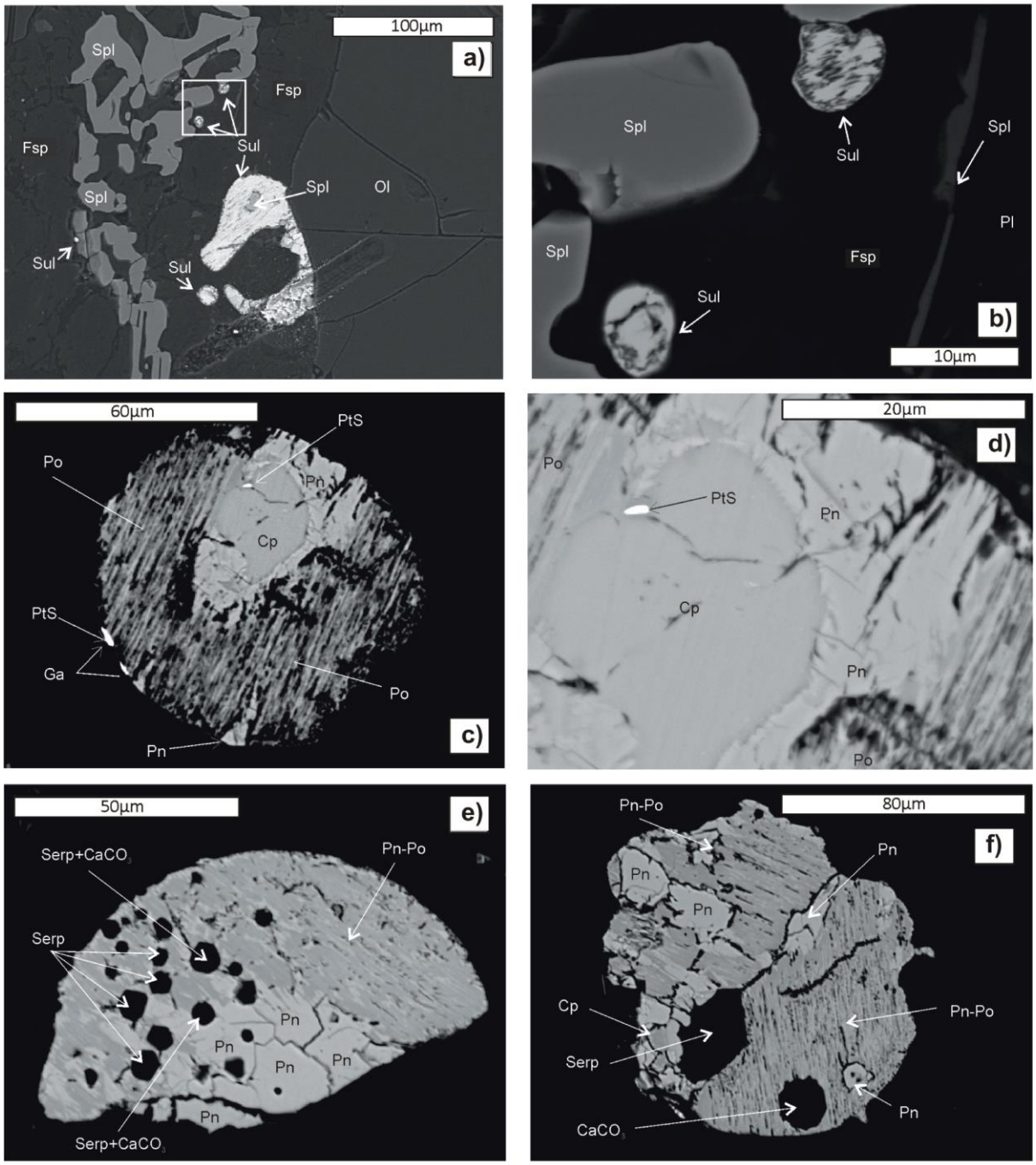

Figure 6

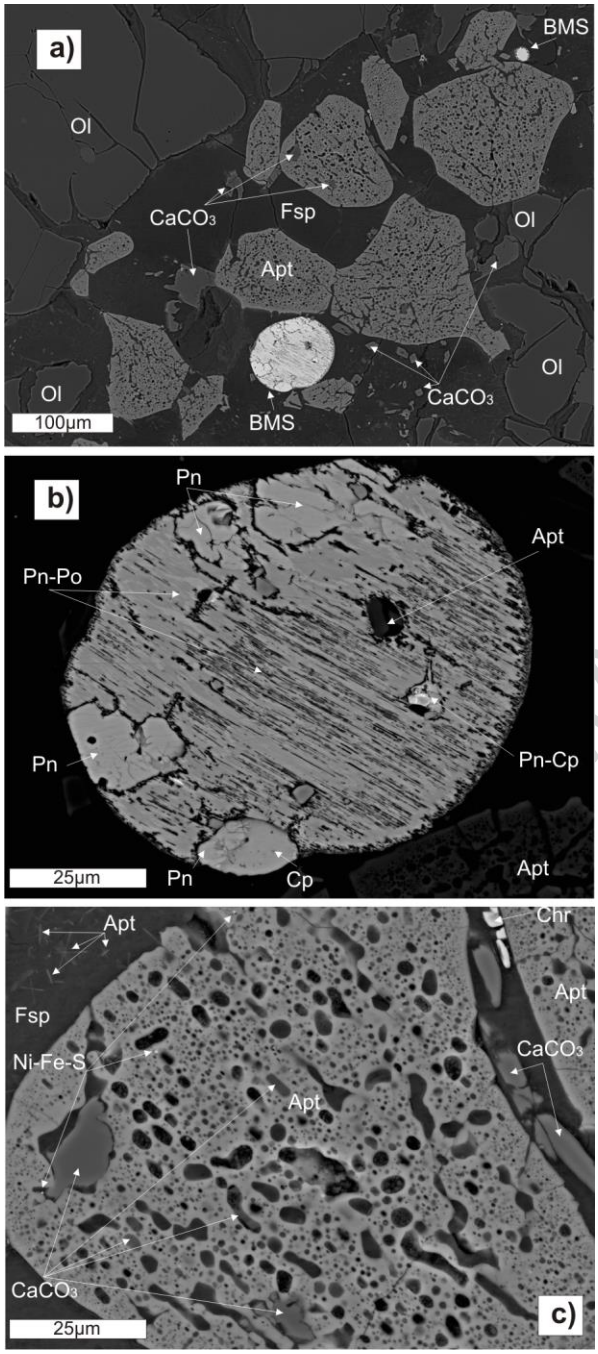

Figure 7

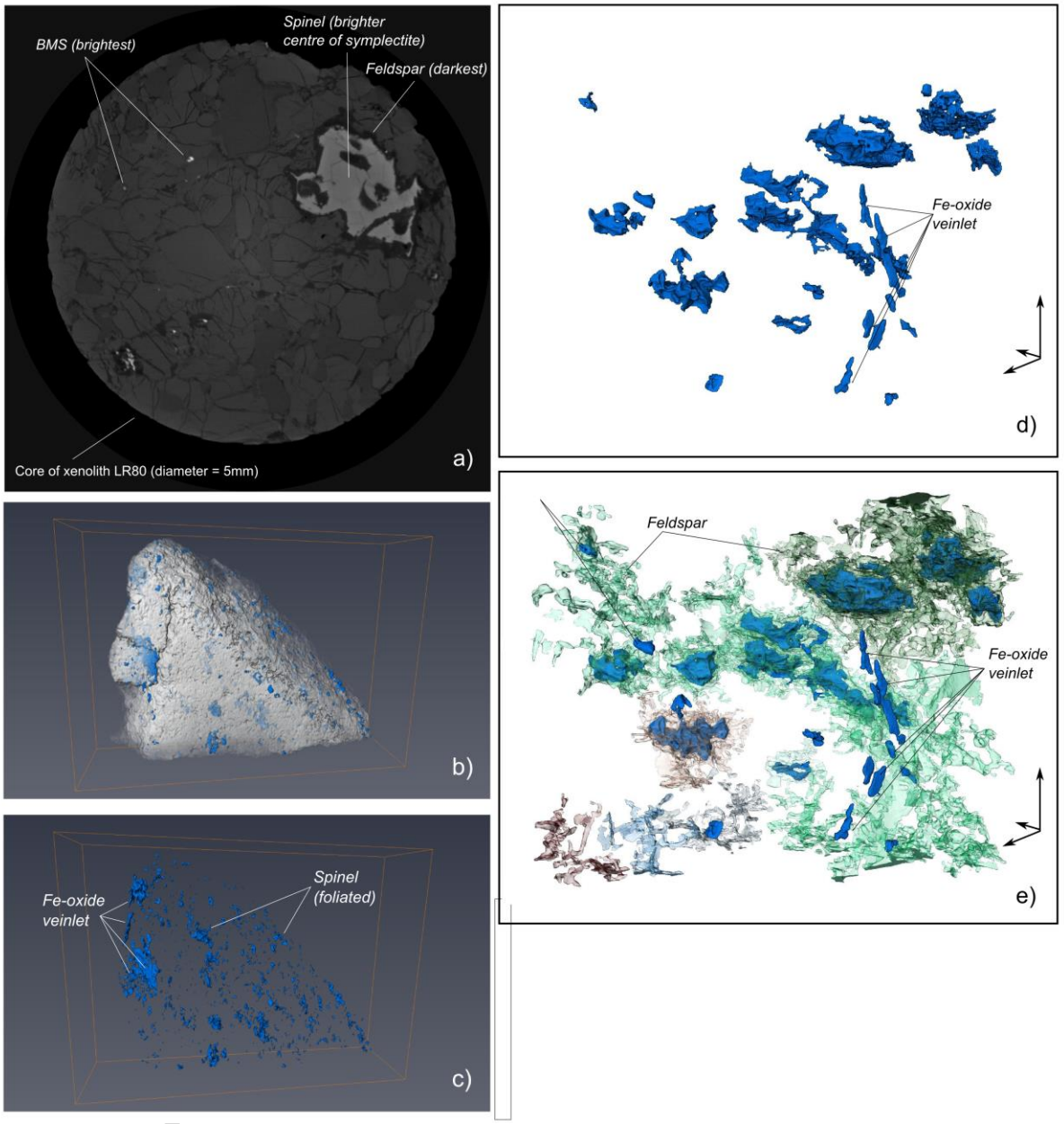

Figure 8

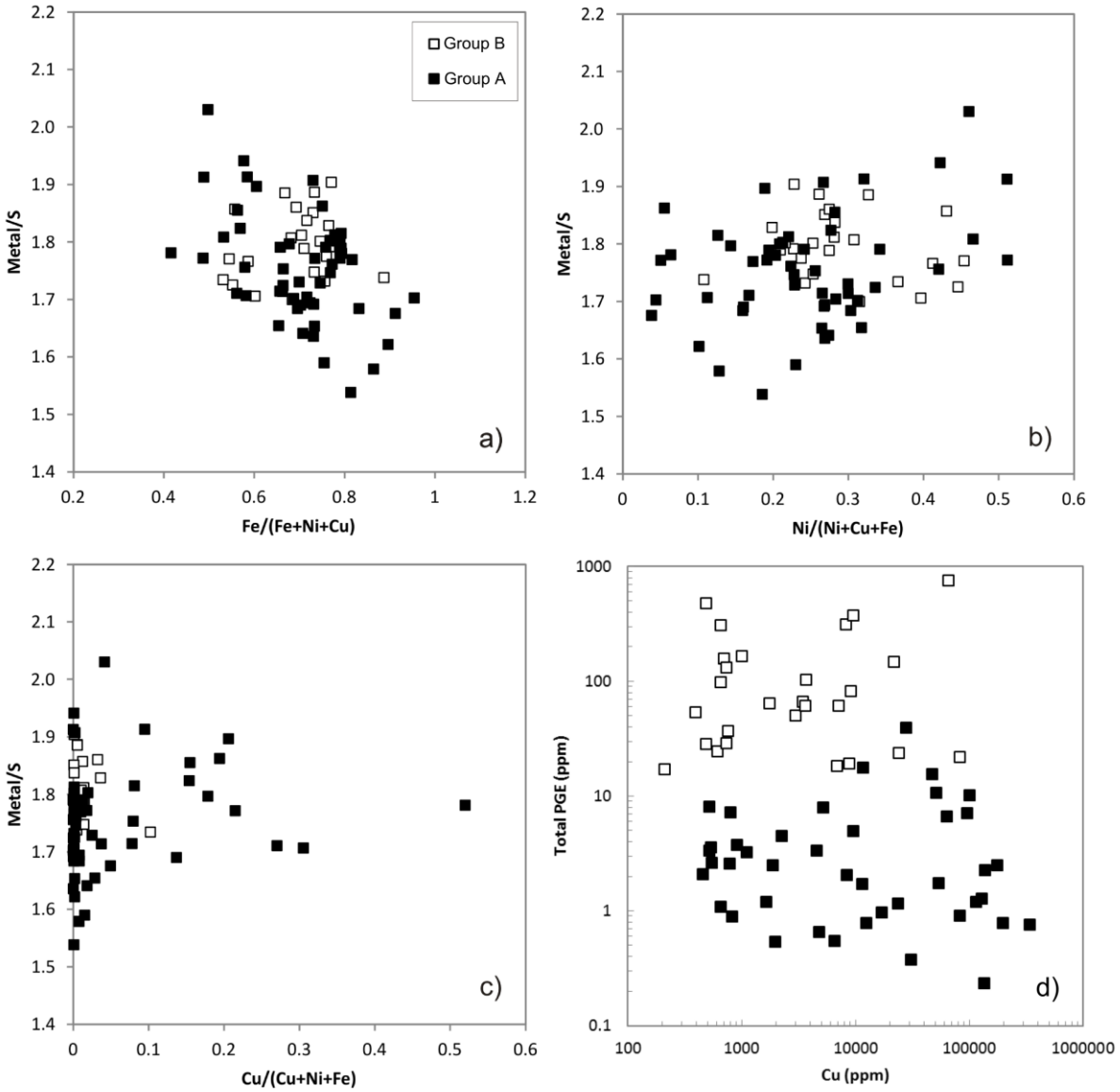

Figure 9

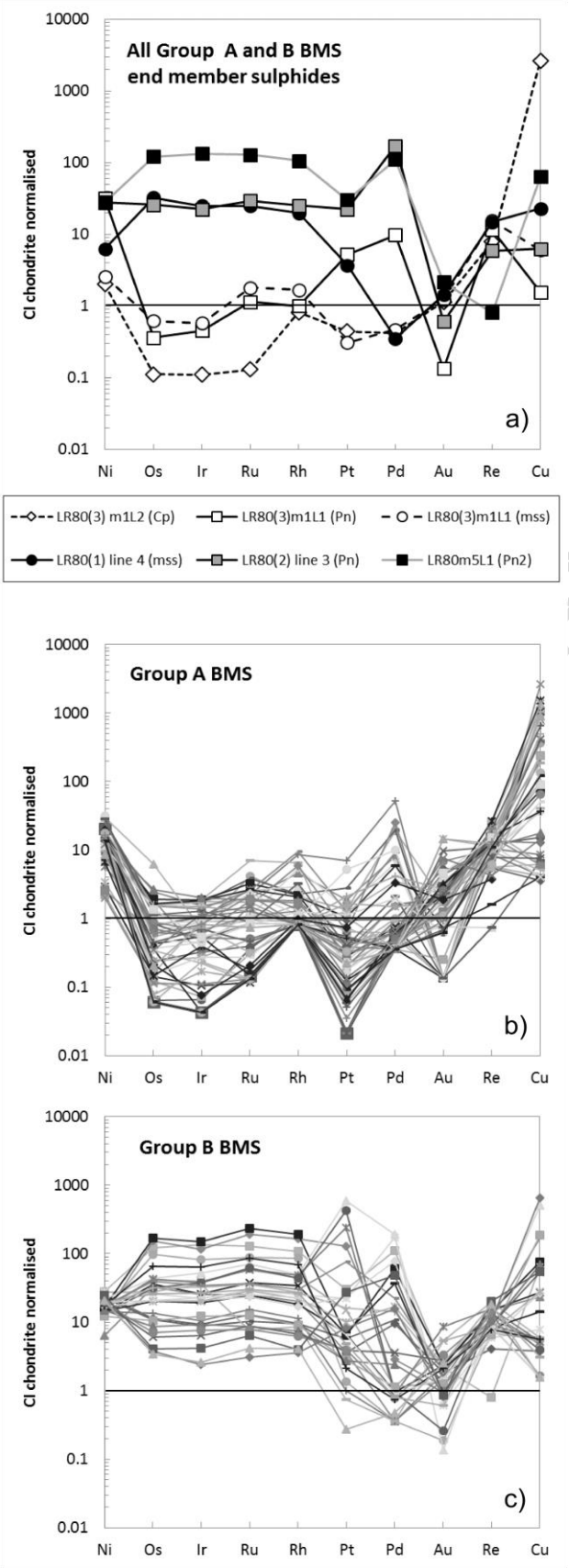

Figure 10

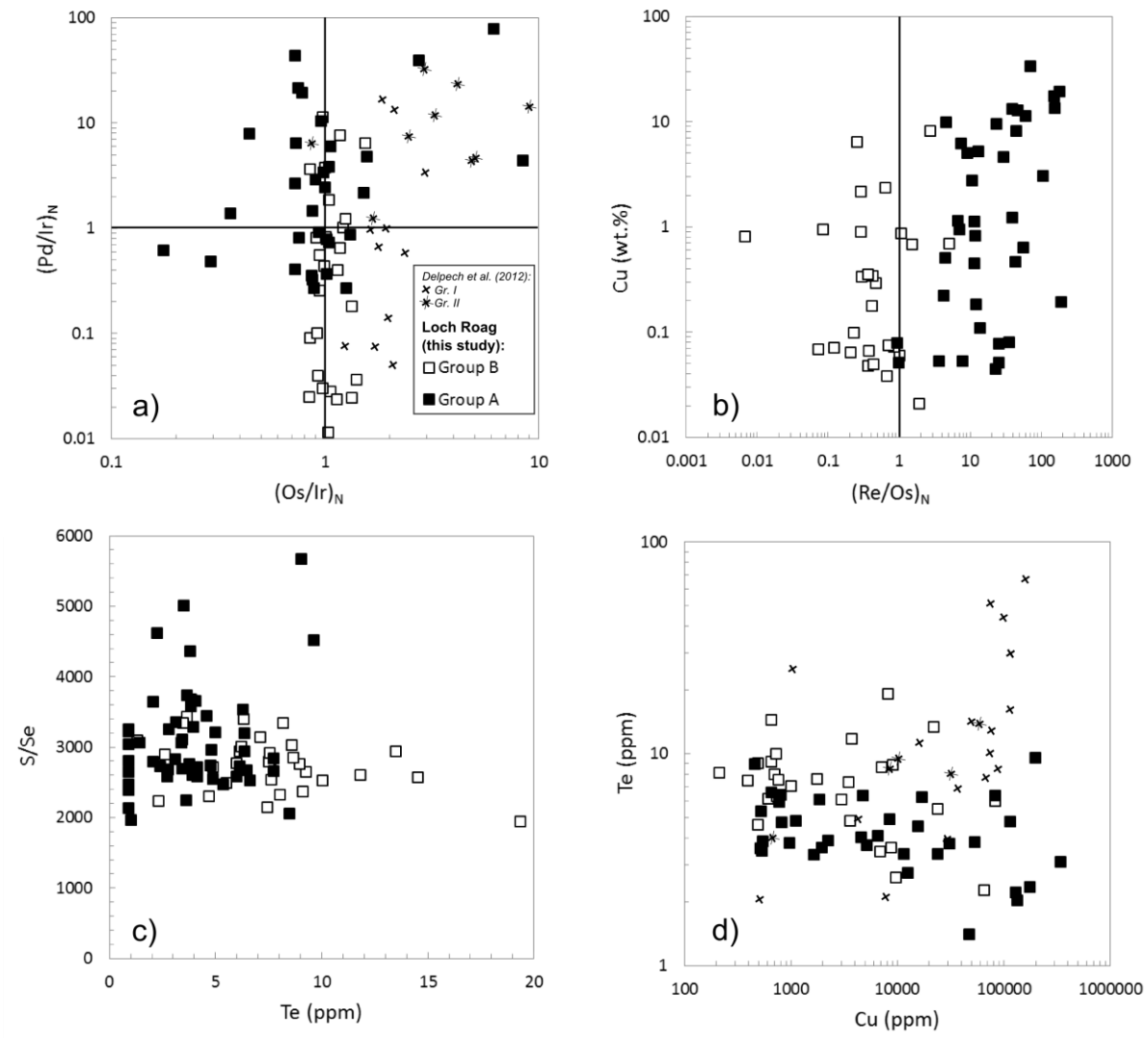

Figure 11

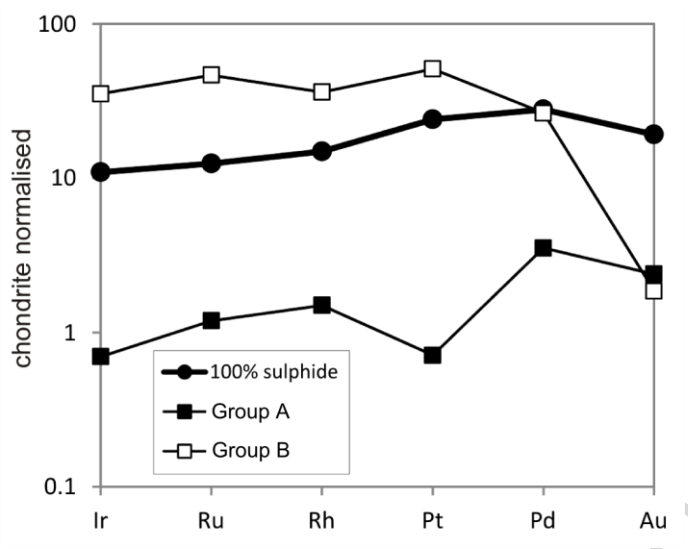

Figure 12

Paradoxical co-existing base metal sulphides in the mantle: the multi-event record preserved in Loch Roag peridotite xenoliths, North Atlantic Craton

Hannah S.R. Hughes[1*], Iain McDonald[2], Matthew Loocke[2], Ian B. Butler[3], Brian G.J. Upton[3], John W. Faithfull[4]

Highlights

- Co-existing populations of base metal sulphide (BMS) in a single mantle xenolith
- Each BMS group has distinct petrographic location, PGE, Re, Se and Te abundances
- The texturally oldest BMS have lowest IPGE concentrations and highest $(Re/Os)_N$ ratios
- The youngest BMS contain PtS, have highest IPGE concentrations and lowest $(Re/Os)_N$
- These IPGE-rich BMS are associated with carbonate-sulphide-phosphate immiscibility